IceCat-1: The IceCube Event Catalog of Alert Tracks

Citation for the original published paper (version of record):
Abbasi, R., Ackermann, M., Adams, J. et al (2023). IceCat-1: The IceCube Event Catalog of Alert Tracks. Astrophysical Journal, Supplement Series, 269(1).
http://dx.doi.org/10.3847/1538-4365/acfa95

The Astrophysical Journal Supplement Series, 269:25 (18pp), 2023 November https://doi.org/10.3847/1538-4365/acfa95

IceCat-1: The IceCube Event Catalog of Alert Tracks

R. Abbasi[1], M. Ackermann[2], J. Adams[3], S. K. Agarwalla[4,65], J. A. Aguilar[5], M. Ahlers[6], J. M. Alameddine[7],
N. M. Amin[8], K. Andeen[9], G. Anton[10], C. Argüelles[11], Y. Ashida[4], S. Athanasiadou[2], S. N. Axani[8], X. Bai[12],
A. Balagopal V[4], M. Baricevic[4], S. W. Barwick[13], V. Basu[4], R. Bay[14], J. J. Beatty[15,16], K.-H. Becker[17],
J. Becker Tjus[18,66], J. Beise[19], C. Bellenghi[20], S. BenZvi[21], D. Berley[22], E. Bernardini[23], D. Z. Besson[24],
G. Binder[14,25], D. Bindig[17], E. Blaufuss[22], S. Blot[2], F. Bontempo[26], J. Y. Book[11], C. Boscolo Meneguolo[23], S. Böser[27],
O. Botner[19], J. Böttcher[28], E. Bourbeau[6], J. Braun[4], B. Brinson[29], J. Brostean-Kaiser[2], R. T. Burley[30], R. S. Busse[31],
D. Butterfield[4], M. A. Campana[32], K. Carloni[11], E. G. Carnie-Bronca[30], S. Chattopadhyay[4,65], N. Chau[5], C. Chen[29],
Z. Chen[33], D. Chirkin[4], S. Choi[34], B. A. Clark[22], L. Classen[31], A. Coleman[19], G. H. Collin[35], A. Connolly[15,16],
J. M. Conrad[35], P. Coppin[36], P. Correa[36], S. Countryman[37], D. F. Cowen[38,39], P. Dave[29], C. De Clercq[36],
J. J. DeLaunay[40], D. Delgado[11], H. Dembinski[8], S. Deng[28], K. Deoskar[41], A. Desai[4], P. Desiati[4], K. D. de Vries[36],
G. de Wasseige[42], T. DeYoung[43], A. Diaz[35], J. C. Díaz-Vélez[4], M. Dittmer[31], A. Domi[10], H. Dujmovic[4],
M. A. DuVernois[4], T. Ehrhardt[27], P. Eller[20], R. Engel[26,44], H. Erpenbeck[4], J. Evans[22], P. A. Evenson[8], K. L. Fan[22],
K. Fang[4], K. Farrag[45], A. R. Fazely[46], A. Fedynitch[47], N. Feigl[48], S. Fiedlschuster[10], C. Finley[41], L. Fischer[2], D. Fox[38],
A. Franckowiak[18], E. Friedman[22], A. Fritz[27], P. Fürst[28], T. K. Gaisser[8], J. Gallagher[49], E. Ganster[28], A. Garcia[11],
L. Gerhardt[25], A. Ghadimi[40], C. Glaser[19], T. Glauch[20], T. Glüsenkamp[10,19], N. Goehlke[44], J. G. Gonzalez[8], S. Goswami[40],
D. Grant[43], S. J. Gray[22], S. Griffin[4], S. Griswold[21], C. Günther[28], P. Gutjahr[7], C. Haack[20], A. Hallgren[19], R. Halliday[43],
L. Halve[28], F. Halzen[4], H. Hamdaoui[33], M. Ha Minh[20], K. Hanson[4], J. Hardin[35], A. A. Harnisch[43], P. Hatch[50],
A. Haungs[26], K. Helbing[17], J. Hellrung[18], F. Henningsen[20], L. Heuermann[28], N. Heyer[19], S. Hickford[17], A. Hidvegi[41],
C. Hill[45], G. C. Hill[30], K. D. Hoffman[22], K. Hoshina[4,67], W. Hou[26], T. Huber[26], K. Hultqvist[41], M. Hünnefeld[7],
R. Hussain[4], K. Hymon[7], S. In[34], A. Ishihara[45], M. Jacquart[4], O. Janik[28], M. Jansson[41], G. S. Japaridze[51], K. Jayakumar[4,65],
M. Jeong[34], M. Jin[11], B. J. P. Jones[52], D. Kang[26], W. Kang[34], X. Kang[32], A. Kappes[31], D. Kappesser[27], L. Kardum[7],
T. Karg[2], M. Karl[20], A. Karle[4], U. Katz[10], M. Kauer[4], J. L. Kelley[4], A. Khatee Zathul[4], A. Kheirandish[53,54],
J. Kiryluk[33], S. R. Klein[14,25], A. Kochocki[43], R. Koirala[8], H. Kolanoski[48], T. Kontrimas[20], L. Köpke[27],
C. Kopper[43], D. J. Koskinen[6], P. Koundal[26], M. Kovacevich[32], M. Kowalski[2,48], T. Kozynets[6], K. Kruiswijk[42],
E. Krupczak[43], A. Kumar[2], E. Kun[18], N. Kurahashi[32], N. Lad[2], C. Lagunas Gualda[2], M. Lamoureux[42], M. J. Larson[22],
F. Lauber[17], J. P. Lazar[4,11], J. W. Lee[34], K. Leonard DeHolton[38,39], A. Leszczyńska[8], M. Lincetto[18], Q. R. Liu[4],
M. Liubarska[55], E. Lohfink[27], C. Love[32], C. J. Lozano Mariscal[31], L. Lu[4], F. Lucarelli[56], A. Ludwig[57], W. Luszczak[15,16],
Y. Lyu[14,25], J. Madsen[4], K. B. M. Mahn[43], Y. Makino[4], E. Manao[20], S. Mancina[4,23], W. Marie Sainte[4], I. C. Mariş[5],
S. Marka[37], Z. Marka[37], M. Marsee[40], I. Martinez-Soler[11], R. Maruyama[58], F. Mayhew[43], T. McElroy[55], F. McNally[59],
J. V. Mead[6], K. Meagher[4], S. Mechbal[2], A. Medina[16], M. Meier[45], Y. Merckx[36], L. Merten[18], J. Micallef[43],
T. Montaruli[56], R. W. Moore[55], Y. Morii[45], R. Morse[4], M. Moulai[4], T. Mukherjee[26], R. Naab[2], R. Nagai[45], M. Nakos[4],
U. Naumann[17], J. Necker[2], M. Neumann[31], H. Niederhausen[43], M. U. Nisa[43], A. Noell[28], S. C. Nowicki[43],
A. Obertacke Pollmann[45], V. O'Dell[4], M. Oehler[26], B. Oeyen[60], A. Olivas[22], R. Orsoe[20], J. Osborn[4], E. O'Sullivan[19],
H. Pandya[8], N. Park[50], G. K. Parker[52], E. N. Paudel[8], L. Paul[9], C. Pérez de los Heros[19], J. Peterson[4], S. Philippen[28],
S. Pieper[17], A. Pizzuto[4], M. Plum[12], A. Pontén[19], Y. Popovych[27], M. Prado Rodriguez[4], B. Pries[43], R. Procter-Murphy[22],
G. T. Przybylski[25], J. Rack-Helleis[27], K. Rawlins[61], Z. Rechav[4], A. Rehman[8], P. Reichherzer[18], G. Renzi[5], E. Resconi[20],
S. Reusch[2], W. Rhode[7], M. Richman[32], B. Riedel[4], E. J. Roberts[30], S. Robertson[14,25], S. Rodan[34], G. Roellinghoff[34],
M. Rongen[27], C. Rott[34,62], T. Ruhe[7], L. Ruohan[20], D. Ryckbosch[60], I. Safa[4,11], J. Saffer[44], D. Salazar-Gallegos[43],
P. Sampathkumar[26], S. E. Sanchez Herrera[43], A. Sandrock[7], M. Santander[40], S. Sarkar[55], S. Sarkar[63], J. Savelberg[28],
P. Savina[4], M. Schaufel[28], H. Schieler[26], S. Schindler[10], B. Schlüter[31], F. Schlüter[5], T. Schmidt[22], J. Schneider[10],
F. G. Schröder[8,26], L. Schumacher[20], G. Schwefer[28], S. Sclafani[32], D. Seckel[8], S. Seunarine[64], R. Shah[32], A. Sharma[19],
S. Shefali[44], N. Shimizu[45], M. Silva[4], B. Skrzypek[11], B. Smithers[52], R. Snihur[4], J. Soedingrekso[7], A. Søgaard[6],
D. Soldin[44], G. Sommani[18], C. Spannfellner[20], G. M. Spiczak[64], C. Spiering[2], M. Stamatikos[16], T. Stanev[8],
T. Stezelberger[25], T. Stürwald[17], T. Stuttard[6], G. W. Sullivan[22], I. Taboada[29], S. Ter-Antonyan[46], M. Thiesmeyer[28],
W. G. Thompson[11], J. Thwaites[4], S. Tilav[8], K. Tollefson[43], C. Tönnis[34], S. Toscano[5], D. Tosi[4], A. Trettin[2], C. F. Tung[29],
R. Turcotte[26], J. P. Twagirayezu[43], B. Ty[4], M. A. Unland Elorrieta[31], A. K. Upadhyay[4,65], K. Upshaw[46],
N. Valtonen-Mattila[19], J. Vandenbroucke[4], N. van Eijndhoven[36], D. Vannerom[35], J. van Santen[2], J. Vara[31],
J. Veitch-Michaelis[4], M. Venugopal[26], S. Verpoest[60], D. Veske[37], C. Walck[41], T. B. Watson[52], C. Weaver[43], P. Weigel[35],
A. Weindl[26], J. Weldert[38,39], C. Wendt[4], J. Werthebach[7], M. Weyrauch[26], N. Whitehorn[43,57], C. H. Wiebusch[28],
N. Willey[43], D. R. Williams[40], A. Wolf[28], M. Wolf[20], G. Wrede[10], X. W. Xu[46], J. P. Yanez[55], E. Yildizci[4], S. Yoshida[45],
F. Yu[11], S. Yu[43], T. Yuan[4], Z. Zhang[33], and P. Zhelnin[11]

[1] Department of Physics, Loyola University Chicago, Chicago, IL 60660, USA
[2] Deutsches Elektronen-Synchrotron DESY, Platanenallee 6, D-15738 Zeuthen, Germany
[3] Dept. of Physics and Astronomy, University of Canterbury, Private Bag 4800, Christchurch, New Zealand

[4] Dept. of Physics and Wisconsin IceCube Particle Astrophysics Center, University of Wisconsin–Madison, Madison, WI 53706, USA; analysis@icecube.wisc.edu
[5] Université Libre de Bruxelles, Science Faculty CP230, B-1050 Brussels, Belgium
[6] Niels Bohr Institute, University of Copenhagen, DK-2100 Copenhagen, Denmark
[7] Dept. of Physics, TU Dortmund University, D-44221 Dortmund, Germany
[8] Bartol Research Institute and Dept. of Physics and Astronomy, University of Delaware, Newark, DE 19716, USA
[9] Department of Physics, Marquette University, Milwaukee, WI, 53201, USA
[10] Erlangen Centre for Astroparticle Physics, Friedrich-Alexander-Universität Erlangen-Nürnberg, D-91058 Erlangen, Germany
[11] Department of Physics and Laboratory for Particle Physics and Cosmology, Harvard University, Cambridge, MA 02138, USA
[12] Physics Department, South Dakota School of Mines and Technology, Rapid City, SD 57701, USA
[13] Dept. of Physics and Astronomy, University of California, Irvine, CA 92697, USA
[14] Dept. of Physics, University of California, Berkeley, CA 94720, USA
[15] Dept. of Astronomy, Ohio State University, Columbus, OH 43210, USA
[16] Dept. of Physics and Center for Cosmology and Astro-Particle Physics, Ohio State University, Columbus, OH 43210, USA
[17] Dept. of Physics, University of Wuppertal, D-42119 Wuppertal, Germany
[18] Fakultät für Physik & Astronomie, Ruhr-Universität Bochum, D-44780 Bochum, Germany
[19] Dept. of Physics and Astronomy, Uppsala University, Box 516, SE-75120 Uppsala, Sweden
[20] Physik-department, Technische Universität München, D-85748 Garching, Germany
[21] Dept. of Physics and Astronomy, University of Rochester, Rochester, NY 14627, USA
[22] Dept. of Physics, University of Maryland, College Park, MD 20742, USA
[23] Dipartimento di Fisica e Astronomia Galileo Galilei, Università Degli Studi di Padova, I-35122 Padova PD, Italy
[24] Dept. of Physics and Astronomy, University of Kansas, Lawrence, KS 66045, USA
[25] Lawrence Berkeley National Laboratory, Berkeley, CA 94720, USA
[26] Karlsruhe Institute of Technology, Institute for Astroparticle Physics, D-76021 Karlsruhe, Germany
[27] Institute of Physics, University of Mainz, Staudinger Weg 7, D-55099 Mainz, Germany
[28] III. Physikalisches Institut, RWTH Aachen University, D-52056 Aachen, Germany
[29] School of Physics and Center for Relativistic Astrophysics, Georgia Institute of Technology, Atlanta, GA 30332, USA
[30] Department of Physics, University of Adelaide, Adelaide, 5005, Australia
[31] Institut für Kernphysik, Westfälische Wilhelms-Universität Münster, D-48149 Münster, Germany
[32] Dept. of Physics, Drexel University, 3141 Chestnut Street, Philadelphia, PA 19104, USA
[33] Dept. of Physics and Astronomy, Stony Brook University, Stony Brook, NY 11794-3800, USA
[34] Dept. of Physics, Sungkyunkwan University, Suwon 16419, Republic of Korea
[35] Dept. of Physics, Massachusetts Institute of Technology, Cambridge, MA 02139, USA
[36] Vrije Universiteit Brussel (VUB), Dienst ELEM, B-1050 Brussels, Belgium
[37] Columbia Astrophysics and Nevis Laboratories, Columbia University, New York, NY 10027, USA
[38] Dept. of Astronomy and Astrophysics, Pennsylvania State University, University Park, PA 16802, USA
[39] Dept. of Physics, Pennsylvania State University, University Park, PA 16802, USA
[40] Dept. of Physics and Astronomy, University of Alabama, Tuscaloosa, AL 35487, USA
[41] Oskar Klein Centre and Dept. of Physics, Stockholm University, SE-10691 Stockholm, Sweden
[42] Centre for Cosmology, Particle Physics and Phenomenology—CP3, Université catholique de Louvain, Louvain-la-Neuve, Belgium
[43] Dept. of Physics and Astronomy, Michigan State University, East Lansing, MI 48824, USA
[44] Karlsruhe Institute of Technology, Institute of Experimental Particle Physics, D-76021 Karlsruhe, Germany
[45] Dept. of Physics and The International Center for Hadron Astrophysics, Chiba University, Chiba 263-8522, Japan
[46] Dept. of Physics, Southern University, Baton Rouge, LA 70813, USA
[47] Institute of Physics, Academia Sinica, Taipei, 11529, Taiwan
[48] Institut für Physik, Humboldt-Universität zu Berlin, D-12489 Berlin, Germany
[49] Dept. of Astronomy, University of Wisconsin–Madison, Madison, WI 53706, USA
[50] Dept. of Physics, Engineering Physics, and Astronomy, Queen's University, Kingston, ON K7L 3N6, Canada
[51] CTSPS, Clark-Atlanta University, Atlanta, GA 30314, USA
[52] Dept. of Physics, University of Texas at Arlington, 502 Yates St., Science Hall Rm 108, Box 19059, Arlington, TX 76019, USA
[53] Department of Physics & Astronomy, University of Nevada, Las Vegas, NV, 89154, USA
[54] Nevada Center for Astrophysics, University of Nevada, Las Vegas, NV 89154, USA
[55] Dept. of Physics, University of Alberta, Edmonton, AB T6G 2E1, Canada
[56] Département de physique nucléaire et corpusculaire, Université de Genève, CH-1211 Genève, Switzerland
[57] Department of Physics and Astronomy, UCLA, Los Angeles, CA 90095, USA
[58] Dept. of Physics, Yale University, New Haven, CT 06520, USA
[59] Department of Physics, Mercer University, Macon, GA 31207-0001, USA
[60] Dept. of Physics and Astronomy, University of Gent, B-9000 Gent, Belgium
[61] Dept. of Physics and Astronomy, University of Alaska Anchorage, 3211 Providence Dr., Anchorage, AK 99508, USA
[62] Department of Physics and Astronomy, University of Utah, Salt Lake City, UT 84112, USA
[63] Dept. of Physics, University of Oxford, Parks Road, Oxford OX1 3PU, UK
[64] Dept. of Physics, University of Wisconsin, River Falls, WI 54022, USA

Received 2023 April 3; revised 2023 September 14; accepted 2023 September 14; published 2023 November 3

---

[65] Also at Institute of Physics, Sachivalaya Marg, Sainik School Post, Bhubaneswar 751005, India

[66] Also at Department of Space, Earth and Environment, Chalmers University of Technology, 412 96 Gothenburg, Sweden

[67] Also at Earthquake Research Institute, University of Tokyo, Bunkyo, Tokyo 113-0032, Japan

Abstract

We present a catalog of likely astrophysical neutrino track-like events from the IceCube Neutrino Observatory. IceCube began reporting likely astrophysical neutrinos in 2016, and this system was updated in 2019. The catalog presented here includes events that were reported in real time since 2019, as well as events identified in archival data samples starting from 2011. We report 275 neutrino events from two selection channels as the first entries in the catalog, the IceCube Event Catalog of Alert Tracks, which will see ongoing extensions with additional alerts. The Gold and Bronze alert channels respectively provide neutrino candidates with a 50% and 30% probability of being astrophysical, on average assuming an astrophysical neutrino power-law energy spectral index of 2.19. For each neutrino alert, we provide the reconstructed energy, direction, false-alarm rate, probability of being astrophysical in origin, and likelihood contours describing the spatial uncertainty in the alert's reconstructed location. We also investigate a directional correlation of these neutrino events with gamma-ray and X-ray catalogs, including 4FGL, 3HWC, TeVCat, and Swift-BAT.

Unified Astronomy Thesaurus concepts: Neutrino astronomy (1100); Astronomical methods (1043); High energy astrophysics (739)

Supporting material: machine-readable table

1. Introduction

The emerging field of multimessenger astronomy combines measurements taken across the electromagnetic spectrum with neutrinos and gravitational waves to elucidate the nature of astrophysical objects. Notable examples of discoveries in recent years include the joint gravitational wave and electromagnetic observation of a binary neutron star merger (Abbott et al. 2017) and the coincident detection of neutrinos and gamma rays from the blazar TXS 0506 + 056 (Aartsen et al. 2018a). Breakthroughs like the latter hold the key to identifying the sites of hadronic acceleration and solving a major open puzzle in modern astrophysics, the origin of cosmic rays. Astrophysical neutrinos are produced in either pp collisions or $p\gamma$ interactions following cosmic-ray acceleration, and neutrino observatories like IceCube have a unique role in probing the distant universe in the TeV–PeV energy regime. The prompt observation of transient phenomena, such as gamma-ray bursts, tidal disruption events, and supernovae, in different wavelengths and messengers requires the rapid sharing of information between different observational facilities. Since 2016, IceCube has been issuing real-time alerts within minutes of the detection of astrophysical neutrino candidates (Aartsen et al. 2017a). Several improvements were introduced in the real-time stream in 2019 (Blaufuss et al. 2020). The updated program includes increased signal purity, better rejection of backgrounds, and an expanded alert selection resulting in more frequent alerts from IceCube than the previous alert program. These improvements also introduced a two-level classification of signal purity in the form of "Gold" and "Bronze" alerts. In this work, we describe the improvements made to the real-time alert selection; apply the updated selection to archival IceCube data going back to 2011, when IceCube first began full operations with 86 strings; and present the first catalog of neutrino events of likely astrophysical origin. This catalog, the IceCube Event Catalog of Alert Tracks (ICECAT-1), contains detailed information on key parameters of 275 neutrino events detected between 2011 May 13 and 2020 December 31, providing a unique sample for multimessenger studies. The accompanying data release provides the log-likelihood sky maps and spatial uncertainties for all events. This will also establish a framework for continued data releases from future alerts, including additions from the most recent IceCube alerts.

This paper is structured as follows. We introduce the IceCube Neutrino Observatory and real-time data selection for this catalog in Section 2. In Section 3, we describe how the alert events are further processed and prepared for follow-ups. We discuss the overall properties of the catalog in Section 4. We describe a potential search for correlations with a few multiwavelength catalogs in Section 5, and we conclude in Section 6.

2. Detector and Event Selection

The IceCube Neutrino Observatory consists of 86 strings of photodetectors embedded in a cubic kilometer of ice beneath the South Pole. The photodetectors, known as digital optical modules (DOMs), are spaced along the vertical length of each string (Abbasi et al. 2009). The strings are arranged on average 125 m apart in a hexagonal grid, with a more densely instrumented set of strings located in the center of the array known as DeepCore (Abbasi et al. 2012). In addition to the in-ice detectors, there is also a surface array of 162 ice-filled tanks instrumented with two DOMs each, known as IceTop (Abbasi et al. 2013). The surface array functions as a detector for air showers induced by cosmic rays and gamma rays.

IceCube detects the Cherenkov light produced by the secondary charged particles from neutrino interactions propagating through the ice. The total number of photoelectrons (PEs) detected (deposited charge) and their arrival times are used to reconstruct the deposited energy and the incoming direction of these charged particles. The optical emission signatures can be classified into two distinct types of event morphologies: tracks and cascades. Track-like events are predominantly produced by muons, which originate in charged-current (CC) interactions of muon neutrinos and from cosmic-ray-induced showers. At the final selection level, the majority of muon-track-like events detected pass fully through the instrumented volume; however, tracks starting or stopping within the instrumented volume are observed. Starting tracks in particular, generated by a muon neutrino CC interaction within the IceCube instrumented volume, can be a strong indication of astrophysical origin (Abbasi et al. 2021a). The directions of such events can be reconstructed with an uncertainty of less than 1° (Aartsen et al. 2014a). The location of the neutrino interaction, which can be $\mathcal{O}$(km) outside the instrumented volume, and the length of the track captured within the detector can lead to large uncertainties in the measured neutrino energy. Cascades are produced by all-flavor neutral-current neutrino interactions, as well as electron-neutrino CC interactions. These events deposit all their energy within spherical showers of $\mathcal{O}(10)$ m and can only be resolved with angular uncertainties of $\sim 10^\circ$ (Aartsen et al. 2014a; Abbasi et al. 2021b). Additionally, cascade-like signatures can arise from CC interactions of tau neutrinos (Aartsen et al. 2020a) or from neutrinos at the Glashow resonance (Aartsen et al. 2021). Tracks—due to their superior angular resolution—are best suited for use in multimessenger searches for astrophysical sources and are the primary constituents of IceCube real-time alerts. In 2020 July, IceCube also began issuing alerts for cascade-like events.[68] However, the cascade sample is not part of the catalog in this paper.

2.1. Real-time Reconstruction and Communication

IceCube detects neutrinos at a rate of a few millihertz, the vast majority of which are atmospheric neutrinos produced in cosmic-ray interactions in Earth's atmosphere (Abbasi et al. 2011; Aartsen et al. 2015). A real-time infrastructure identifies events with a significant probability of being of astrophysical origin (neutrino energy $> \sim 100$ TeV) and promptly alerts the astronomy community to such a detection. The system is described in detail in Aartsen et al. (2017b). We discuss it briefly here, with an emphasis on updates and improvements relevant for this catalog.

An online filtering system at the South Pole identifies candidate neutrino events. The candidate events are reconstructed on several hundred parallel filter clients to determine their observed energies, directions, and morphology. Additional selection criteria (Aartsen et al. 2017b) are applied to determine whether an event passes the preliminary online alert criteria. A single online alert writer process collates these events for transmission to I3Live—the IceCube experiment control system (Aartsen et al. 2017a). The key event summary data for candidate events passing the quality cuts are relayed to the IceCube data center in the Northern Hemisphere over satellite. The full event information, including the signals registered by the DOMs, follows in a second message that is used for a detailed follow-up reconstruction as explained in Section 3.

A dedicated computing system, located at the IceCube data center in the Northern Hemisphere, further evaluates the alert candidates arriving from the South Pole to check whether they pass the online alert criteria. If selected, an alert message is generated and distributed to the public through the Astrophysical Multimessenger Observatory Network system (Ayala Solares et al. 2020), which utilizes the General Coordinates Network[69] (GCN) for communication. The whole chain of events, from the neutrino detection to the issuance of an alert, is fully automated and takes between 30 and 40 s on average.

2.2. Updated Event Selections

The updated event selection introduced in 2019 includes two key improvements that aim to convey the detection of potential astrophysical tracks to the community as frequently as possible. One is the introduction of "Gold" and "Bronze" streams that classify alerts based on their likelihood of being astrophysical in nature. The classification is based on a quantity called "signalness," which is defined as

$$\text{Signalness}(E, \delta) = \frac{N_{\text{signal}}(E, \delta)}{N_{\text{signal}}(E, \delta) + N_{\text{background}}(E, \delta)}. \quad (1)$$

Here E is the reconstructed event energy, δ is the event decl., and $N_{\text{signal}}(E, \delta)$ and $N_{\text{background}}(E, \delta)$ are the expected number of signal and background events at decl. δ and above energy E determined from simulations. $N_{\text{signal}}(E, \delta)$ and $N_{\text{background}}(E, \delta)$, and therefore signalness, are functions of the assumed astrophysical neutrino spectrum. The streams were optimized on simulations using an astrophysical neutrino spectrum of $E^{-2.19}$ (Haack & Wiebusch 2017). The signalness quantity assigns a probability of being an astrophysical neutrino to each alert event, assuming the same $E^{-2.19}$ astrophysical neutrino spectrum. The alert generation criteria are optimized such that "Bronze" alerts have an average signalness value between 30% and 50%, whereas "Gold" candidates have an average signalness above 50%. Thus, the Gold stream has a higher signal purity. We note that the signalness is calculated after event selection to grade alerts and is not explicitly used in alert selection. Certain tracks with high signalness values may not pass the real-time criteria and would end up in other selections. The signalness of each alert is sent out as part of the GCN notice. The "notice type" field indicates the Bronze (Gold) alerts as ICECUBE Astrotrack Bronze (Gold). An example of a GCN notice for IC190730A can be seen at https://gcn.gsfc.nasa.gov/notices_amon_g_b/132910_57145925.amon.

The second improvement to the updated event selection is the introduction of a new track selection known as gamma-ray follow-up (GFU) selection. This complements the previously existing selections in the real-time scheme. The event selections are summarized below.

2.2.1. Gamma-Ray Follow-up Event Selection

This event selection is based on an existing IceCube data neutrino candidate selection that was originally designed to provide triggers for follow-up by Imaging Air Cherenkov Telescopes in gamma rays—hence the name GFU (Aartsen et al. 2016a). This reconstruction targets through-going tracks and employs separate boosted decision-tree-based selections for events from the Northern and Southern Hemispheres (up-going and down-going events in the IceCube reference frame, respectively) to suppress atmospheric backgrounds. A threshold is applied to the reconstructed event energy to achieve the 30% and 50% signalness criteria for alerts. This results in only the highest-energy events (hundreds of TeV) being selected. Figure 1 shows the effective area for the GFU Gold and Bronze alert selection as a function of neutrino energy. The majority (86%) of the alerts issued by IceCube fall under the GFU selection. The 10 yr catalog includes 72 GFU Gold and 164 GFU Bronze events.

2.2.2. High-energy Starting Event Selection

The high-energy starting event (HESE) selection for alerts includes only starting tracks, track-like events that have the neutrino interaction vertex inside the fiducial volume of the detector (Abbasi et al. 2021a). This technique efficiently rejects the atmospheric muon background (Aartsen et al. 2013). Since the highest-energy events are more likely to be of astrophysical

---

[68] https://gcn.gsfc.nasa.gov/amon_icecube_cascade_events.html

[69] https://gcn.nasa.gov/

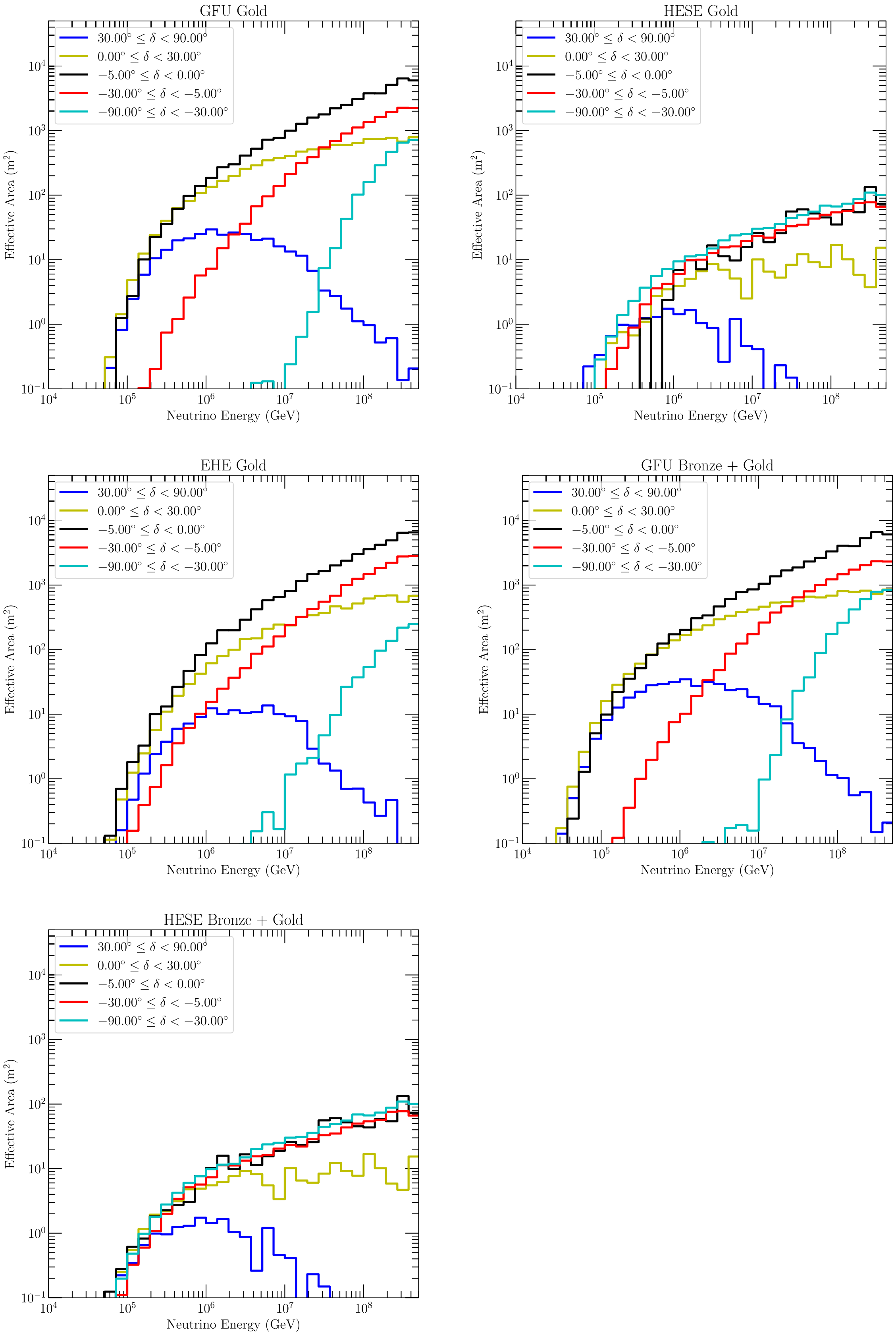

Figure 1. The $\nu_\mu + \bar{\nu_\mu}$ effective areas for the event selections used in this catalog as a function of neutrino energy. The solid lines show the effective area in different decl. bands: [30°, 90°] (blue), [0°, 30°] (yellow), [−5°, 0°] (black), [−30°, −5°] (red), and [−90°, −30°] (cyan).

origin, only the events that have a total deposited charge in the detector of at least 6000 PEs are considered. As an improvement to previous HESE alerts (Aartsen et al. 2017b), additional cuts are introduced to further reduce poorly reconstructed events. We only use events that have a minimum measured track length of 200 m. Due to the effective veto

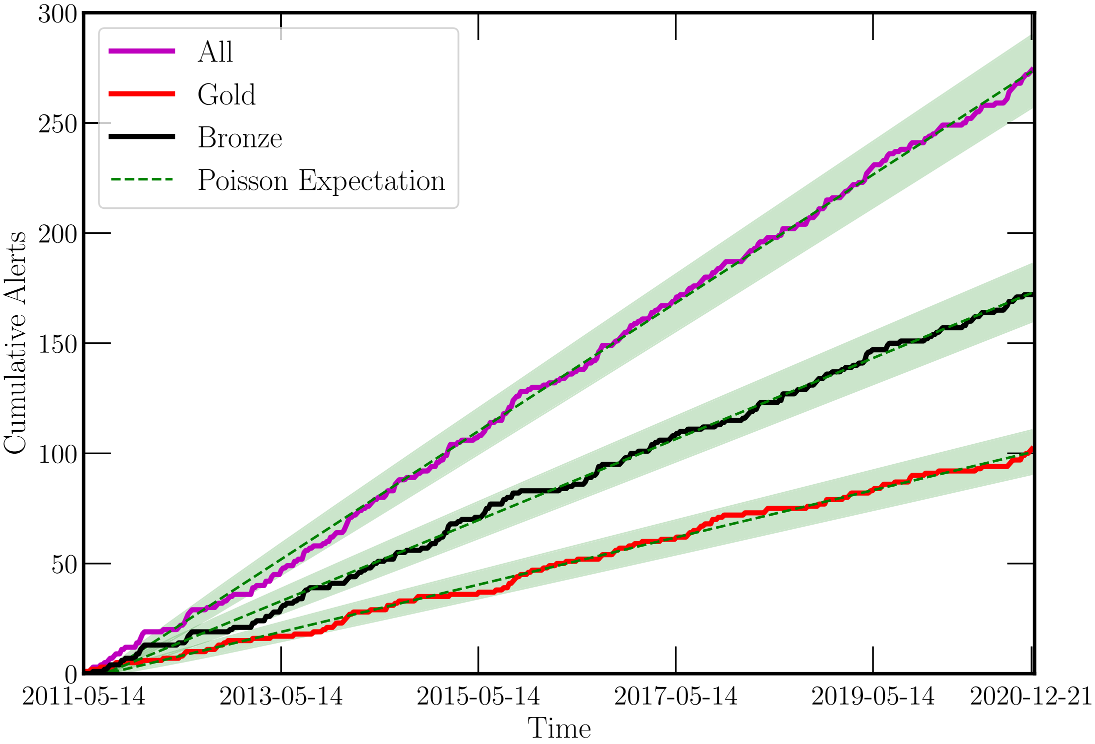

Figure 2. The cumulative number of alerts as a function of time. The solid black and red lines show the number of Gold and Bronze alerts, respectively, while the magenta line shows the combined number for all alerts. The dashed green line and the shaded green band show the median and standard deviation, respectively, of the best-fit Poisson distribution to the number of alerts in each category.

Table 1
The Number of Expected Signal and Background Events, and the Total Observed Events for Each Alert Stream in ∼9.6 yr of the Catalog Live Time

Event Type	Expected Signal	Expected Background	Total Expected	Total Observed
GFU Gold	54.3	47	101.3	72
GFU Bronze	40.2	138	178.2	164
HESE Gold	5.3	4	9.3	9
HESE Bronze	1.6	9	10.6	8
EHE Gold	3.9	19	22.9	22

Note. The expected number of events is calculated for the best-fit diffuse muon neutrino flux (Abbasi et al. 2022a) with a spectral index of 2.37.

requirement for HESE alerts, down-going events from the Southern Hemisphere can be observed at lower neutrino energies, as illustrated by the HESE effective area for different decl. bins in Figure 1. The 10 yr catalog includes nine HESE Gold and eight HESE Bronze events.

2.2.3. Extremely High Energy Event Selection

The extremely high energy event (EHE) selection is optimized for detecting track-like neutrino events with energies between 500 TeV and 10 PeV. Atmospheric backgrounds are minimized by employing a two-dimensional cut in the plane of the reconstructed zenith angle and the logarithm of the deposited charge detected. The selection is unchanged from the one described in Aartsen et al. (2017b), and the cuts are set to achieve an average signalness of 50%, and therefore EHE events are only sent as part of the Gold stream. Figure 1 shows the effective area for the EHE selection as a function of neutrino energy. This catalog contains 22 events that passed the EHE selection during the 9.6 yr period.

2.3. Expected and Observed Rates

Figure 2 shows the time evolution of the number of observed alerts over the years. The cumulative number of total alerts, as a function of year, is best described by a straight line with slope 28.6 alerts yr^{-1}. Table 1 shows the number of expected and observed events in the 3514 days of the IceCube data used in this work. We calculate the expected number of alerts arising from astrophysical sources for each selection by multiplying its respective effective area with IceCube's latest measured diffuse astrophysical muon neutrino spectrum (Abbasi et al. 2022a), which reports a spectral power-law index of 2.37. Since the event selection was originally optimized assuming a spectral index of 2.19 based on a previous IceCube measurement (Haack & Wiebusch 2017), the numbers reported here slightly differ from the ones in Blaufuss et al. (2020). IceCube continues to take data and refine its reconstruction methods, resulting in a more precise measurement of the astrophysical neutrino spectrum over the years. This evolution is reflected in the use of an updated spectral index in this work. The expected number of signal events can change up to ∼15% when using a spectral index of 2.19 instead of 2.37. The expected number of background events is calculated using a simulation of atmospheric muons and neutrinos (Heck et al. 1998; Schönert et al. 2009). We also note that the event selections are not mutually exclusive—a single event may pass multiple selections. In particular, GFU and EHE selections have significant overlap, as they both focus on through-going tracks. The expected numbers in Table 1 account for the overlap and only report the unique events from each stream. In real time, if an event passes multiple selections, only one alert is issued based on a hierarchical rule for labeling. The hierarchical scheme in order of preference for the Gold stream is GFU Gold, EHE Gold, and HESE Gold. Similarly, for the Bronze stream, a GFU Bronze alert is sent preferentially over an HESE Bronze alert. An event passing both the Gold and Bronze selections is only sent in the Gold stream. The preference order is decided based on the angular resolutions and relative signal purity of the different streams.

The observed rates of alerts from the Gold and Bronze channels shown in Table 1 are compatible with expectations when considering Poisson fluctuations, as well as the uncertainties in the astrophysical neutrino spectral parameters and the background modeling. For instance, considering the errors on the measured diffuse muon neutrino spectral parameters (Abbasi et al. 2022a), the expected number of GFU Gold signal events can be as low as 39.1, bringing the overall expected rate from 101.3 to 86.1, which is within $\sim 1.5\sigma$ of the observed number of 72 events. It should be noted that while the average signalness of the Gold and Bronze selection, as shown in Figure 5, generally agrees with the 50% and 30% targets, the overall mix of signal and background events is different. This arises from the differing signal and background energy distributions near the selection threshold. Overall, the HESE Gold stream has the highest average signal purity of ~57%.

In addition to overall rates for each alert type, we also calculate the false-alarm rate (FAR) on an event-by-event basis. The FAR for a given alert gives the annual rate of background events in IceCube with a direction and energy similar to the issued alert and is derived from $N_{\mathrm{background}}(E, \delta)$ used in the signalness calculation.

3. Alert Processing and Follow-ups

Due to computational limitations at the South Pole experimental site and the need for promptly issuing an alert, the online reconstruction cannot utilize complex, computationally intensive algorithms. Once all the event information has been transmitted to the north, a more refined set of follow-up reconstructions based on Aartsen et al. (2014a) begin on a computing cluster. The follow-up reconstruction consists of a maximum-likelihood-based scan of the entire sky to search for an event direction consistent with the signals registered by the DOMs. We bin the sky into two-dimensional grids of increasing resolution in steps following the HEALPix pixelization scheme (Górski et al. 2005). Each pixel defines a potential event direction in R.A. and decl. At each step, in each pixel, we fix the event direction and compute the likelihood of the best-fit deposited energy and the neutrino interaction position. Repeating the procedure over all pixels yields a likelihood map of the sky. The pixel corresponding to the maximum likelihood defines the best-fit direction of the neutrino event. The scans are first performed on a coarse grid with NSIDE = 8, corresponding to a mean pixel spacing of $7\overset{\circ}{.}3$. The best-fit pixels are selected for the next steps with finer scans with NSIDES 64 (pixel size $0\overset{\circ}{.}9$) and 1024 (pixel size $0\overset{\circ}{.}06$). Each sky scan takes from 1 to 3 hr, yielding an improved angular reconstruction over the initial alert. In order to ensure that the reconstruction converges to a global minimum, at each step we test several positional variations iteratively by using the result of a regular fit as a seed for the next iteration. If there are multiple local minima, the repeated iterations ensure that at least one of the results is a global minimum.

The angular uncertainty contours at 50% and 90% confidence level are extracted using predefined values of change in log-likelihood based on simulated neutrino events to ensure the required coverage (Aartsen et al. 2018b). In order to cover potential systematic errors from detector uncertainties (such as glacial ice optical parameters), the detector systematic parameters were varied within expected errors during the simulation of the neutrino events used to determine the contour levels. As described in Aartsen et al. (2018b), we simulate an ensemble of events with similar energy deposition and position in the detector to those of IC160427A (Kankare et al. 2019), varying the ice model parameters (Abbasi et al. 2022b) in each simulation. The simulated events are reconstructed, and the log-likelihoods of their reconstructed directions are compared to the log-likelihoods of their true directions. This procedure yields a distribution of change in log-likelihood that folds in the systematic uncertainties and is used to extract the error contours. We note that the calibration of the change in log-likelihood is especially sensitive to the optical properties of the ice, an area of intense study within IceCube (Abbasi et al. 2021c). While these results represent our current modeling, updated parameters and reconstructions for alert candidates will be released as catalog updates as they become available. In real-time operations, the results from the follow-up scan are disseminated via a GCN circular and a revised GCN notice. In particular, the notice includes the circularized error region based on the follow-up reconstruction. An example of the revised GCN notice for the event IC190730A can be seen at https://gcn.gsfc.nasa.gov/gcn3/25225.gcn3.

For the compilation of the catalog, the same sky scan is performed on the selected alerts from the archival IceCube data on a commercial cloud computing service. Figure 3 illustrates the result of one such scan, for an example alert from the catalog, IC150119. In addition, we also apply a convolutional neural network (CNN) based classifier to better distinguish the morphology of each event (Kronmueller & Glauch 2019). Each event is assigned a score between 0 and 1 for how well it fits the following four hypotheses: cascade, skimming event (primary vertex outside the detector and no energy deposited within), starting track (interaction vertex inside the detector volume), or stopping track (track length of less than ~1500 m). In this work, we provide the complete likelihood maps and the uncertainty contours, as described above, for all the alerts in the accompanying data release.

3.1. IceTop Veto

Recently, on 2022 October 21, we introduced an additional veto mechanism to reject atmospheric muons that may pass the alert selection criteria. This veto makes use of the IceTop surface array to search for cosmic-ray-induced showers accompanying a track-like event in the in-ice detector (Amin 2021). This is particularly useful in the case of down-

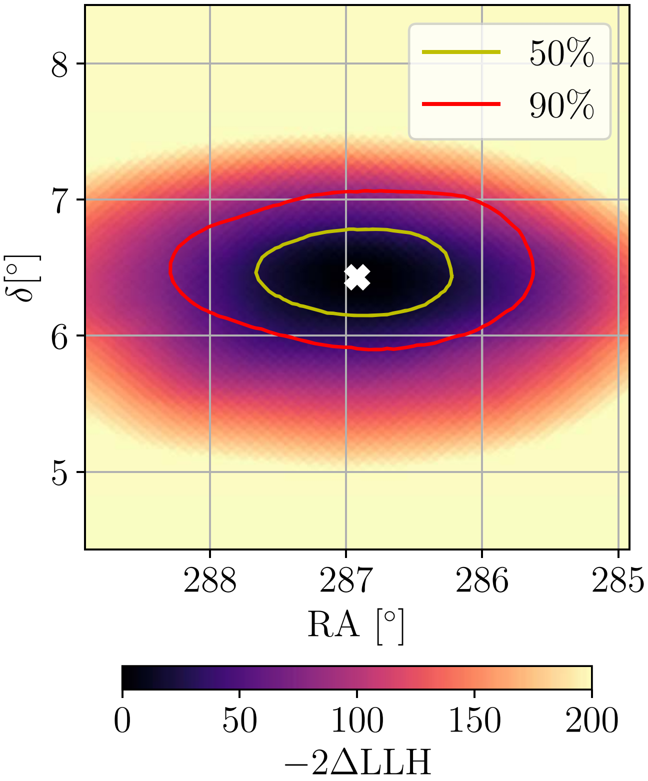

Figure 3. The result of the sky scan shown in likelihood space for IC150119. The best-fit position of the event is noted by the white cross in the center where the likelihood is maximized. The yellow and red contours denote the uncertainty in the location as the 50% and 90% confidence level changes in the likelihood, respectively (see Section 3). A rectangle that contains the 90% error contour is used to report the +/- errors on the alert location (see Table 2).

going air showers inclined at an angle, typically below 82° with respect to the zenith, that pass through IceCube and where the reconstructed track is not fully contained in the IceTop detector footprint. The IceTop veto criteria look for a threshold number of coincident pulses in IceTop tanks during a 1 μs time window (Amin 2021). Since the criteria were developed after the compilation of the catalog, we do not discard the vetoed alerts but mark them as such. The probability that the veto algorithm incorrectly rejects a true astrophysical neutrino event is $\sim 10^{-4}$.

4. Catalog Properties

We compile the neutrino alert catalog by applying the abovementioned procedures of event selection followed by likelihood scans on IceCube data going back to 2011 May. A total of 275 events pass the alert criteria through the end of 2020, including alerts issued in real time after the updated system was activated in 2019 June. Figure 4 shows the location of all the alerts on a sky map in equatorial coordinates. Figure 6 shows the distribution broken down by alert type. The breakdown of the number of alerts by stream and selection is shown in Table 1. Figure 5 shows the distributions of energies, FARs, and signalness parameters for all the alerts. Table 2 shows all alerts with their best-fit directions and 90% uncertainties (J2000 coordinates), energy (assuming a spectral index of 2.19), and signalness information. The probable neutrino energy for each event is calculated from the observed muon energy (Abbasi et al. 2013). Figure 7 illustrates the spread of true neutrino energies that contribute to a given observed muon energy. The uncertainties on alert directions reported in Table 2 are obtained from the rectangular region bounding the error contours. After the construction of the catalog, we also checked data from IceTop for signatures of cosmic-ray activity that is temporally correlated with each of the alerts. Eight alerts were vetoed by IceTop data as described above. Such alerts are likely to be caused by atmospheric background and are marked with an asterisk in Table 2, but as these veto criteria were added at a later time, these events were not removed from the catalog. These vetoed events are likely not of astrophysical origin, and future real-time alerts will not be issued for events that fail these veto criteria.

The neutrino event selection used in this catalog is designed to select astrophysical event candidates that are likely to provide well-reconstructed directions on the sky. However, this is not the only astrophysical event selection to have been used in IceCube, and several historical catalogs of astrophysical neutrino candidates have been previously released (Aartsen et al. 2014b, 2016b, 2018b; Abbasi et al. 2022a). While several events contained in these previous catalogs are included here, several do not meet the selection criteria used for this real-time alert selection. This does not imply that these events are not potential astrophysical neutrino candidates, but rather that automated event selections cannot supply sufficient information to issue alerts automatically. The information included here for these events also represents our updated understanding of these candidates, using the latest calibration, glacial ice modeling, and reconstruction algorithms.

The complete catalog is provided in electronic format on Harvard Dataverse at doi:10.7910/DVN/SCRUCD, with columns in addition to the ones in Table 2 for each event as follows: `I3TYPE` (event selection type), `FAR` per year, scores for each CNN classification for event topology, and a `CR_VETO` flag to mark significant temporally coincident cosmic-ray shower activity with a given alert.

5. Search for Correlations with Potential Candidates for Association

Once an IceCube alert is issued, telescopes can begin follow-up observations around the best-fit location of the neutrino event for potential electromagnetic counterparts. Sources lying within the angular uncertainty contours can be probed on different timescales for transient activity to obtain clues as to the origin of the neutrino. Using a variety of data samples, IceCube continues to conduct searches for long-term neutrino emission and for correlations of neutrino data with known astrophysical objects across different wavelengths (Aartsen et al. 2017c, 2019, 2020b; Abbasi et al. 2022c). For the 275 neutrino events in this catalog, we are performing several follow-up analyses that are the subject of ongoing and recent publications (Abbasi et al. 2023a, 2023b). In this work, we report the results of a time-independent search for spatial correlations between the best-fit positions of the alerts and of sources from five catalogs of gamma-ray and X-ray sources.

We use the following catalogs: the 4FGL-DR2 (Abdollahi et al. 2020) and 3FHL (Ajello et al. 2017) catalogs from Fermi-LAT, the 3HWC catalog (Albert et al. 2020) from the HAWC observatory, TeVCat (Wakely & Horan 2008), and the Swift-BAT catalog of hard X-ray sources (Oh et al. 2018). We note that these catalogs are not completely independent, and some of the sources are present in multiple catalogs. For each of the 275 alerts, using the aforementioned catalogs, we search for sources that lie within the 90% uncertainty contour of the alert's

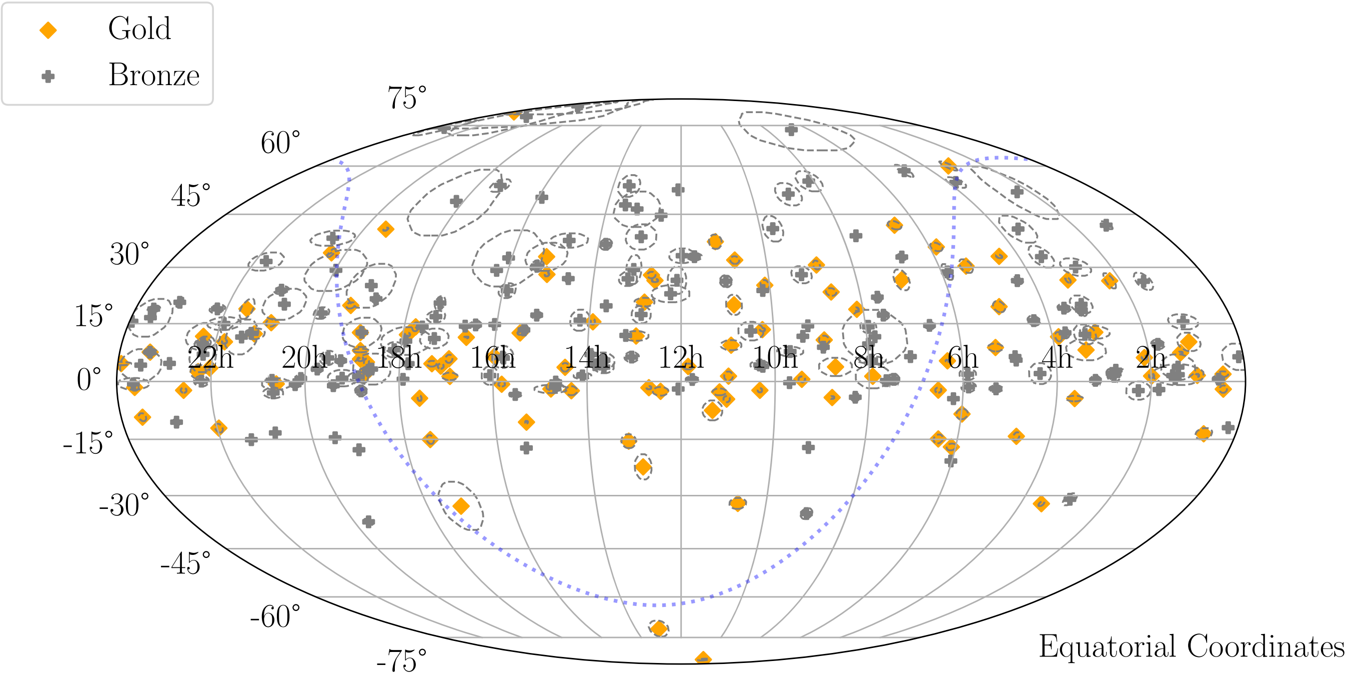

Figure 4. The all-sky distribution of the alerts in the catalog in equatorial coordinates. The orange diamonds show the Gold alerts. The gray crosses show the Bronze alerts. The 90% uncertainty contours at the location of each alert are shown by the dashed ellipses.

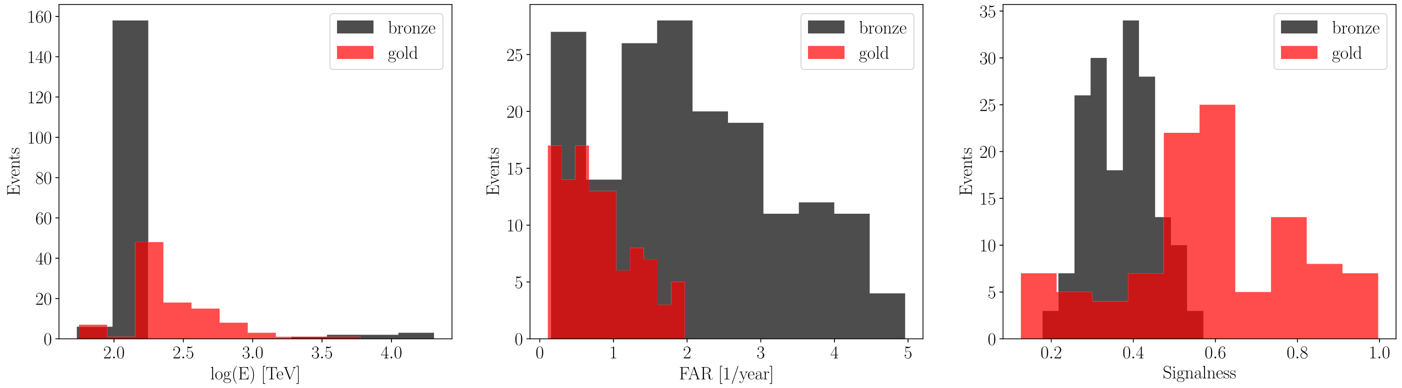

Figure 5. Left: the logarithmic distribution of likely neutrino energies (assuming a spectral index of 2.19) in TeV for the catalog. Middle: the distribution of the FAR of the alerts in the catalog. Right: the distribution of signalness of the alerts in the catalog. The red (gray) histogram shows the Gold (Bronze) alerts.

reconstructed direction. For all sources found within the error contour of a given alert, we calculate their angular distance from the best-fit location of the alert. The closest source and its distance from the best-fit location of the alert are reported in Table 2. We find that 139 neutrino alerts have no source from any of the above catalogs in the uncertainty region. For each of the five catalogs, we also determine the total number of alerts that are spatially coincident with at least one source in the catalog. We also determine how many such coincidences are expected due to chance by randomizing the alert directions in R.A. 1000 times and looking at the number of coincidences after each randomization. The sensitivity of IceCube is approximately uniform as a function of R.A. The randomization allows the production of simulated data with the characteristics of the null hypothesis (no correlation with the catalogs). For each catalog, we find that the number of coincidences is consistent with the median expectation due to chance. The number of observed correlations and the median number expected due to chance for each catalog are shown in Table 3.

Five Fermi-LAT sources—4FGL J0914.1–0202, 4FGL J1019.7+0511, 4FGL J2226.6+0210, 4FGL J2227.9+0036, and 4FGL J0244.7+1316—and one Swift-BAT source, SWIFT J2235.7+013, appear to be spatially correlated with more than one alert and are considered as repeated candidates for association. The correlations, however, are not unique, as there are often multiple sources located within an error contour. Moreover, such repeated associations are not uncommon in randomized R.A. data sets. For 4FGL alone, we observe on average four candidates for repeated associations in 1000 simulations. We emphasize that spatial correlations between neutrino alerts and sources from other catalogs are not evidence for definitive association, as the observed number of correlations is consistent with accidental correlations, as shown above. However, we encourage dedicated follow-up studies using the light curves of the closest sources to each alert identified in this study.

Table 2
Alert Events in the Catalog, Along with Their Time, Positions, Energy, Signalness, and the Closest Source within the Alert Error Contours from the Spatial Correlation Search

Alert	MJD	R.A. (deg)	Decl. (deg)	Energy (TeV)	Signalness	Nearest Source (deg)
IC110514A	55,695.064	$138.47^{+6.68}_{-3.78}$	$-1.94^{+0.97}_{-1.12}$	187	0.51	4FGL J0914.1–0202 (0.12)
IC110610A	55,722.426	$272.55^{+1.67}_{-2.42}$	$35.64^{+1.30}_{-1.05}$	294	0.75	4FGL J1808.8+3522 (0.37)
IC110616A	55,728.730	$71.15^{+1.41}_{-2.07}$	$5.38^{+0.79}_{-0.90}$	109	0.26	... (...)
IC110714A	55,756.113	$68.20^{+0.31}_{-1.10}$	$40.67^{+0.44}_{-0.44}$	72	0.78	... (...)
IC110726A	55,768.511	$151.08^{+1.19}_{-1.71}$	$6.99^{+0.98}_{-0.83}$	160	0.40	... (...)
IC110807A	55,780.980	$336.80^{+1.36}_{-1.98}$	$1.53^{+0.93}_{-0.78}$	108	0.27	4FGL J2226.6+0210 (0.65)
IC110818A	55,791.689	$332.45^{+0.97}_{-1.23}$	$-2.09^{+0.93}_{-0.90}$	123	0.34	... (...)
IC110902A	55,806.092	$9.76^{+2.86}_{-1.32}$	$7.59^{+0.87}_{-0.86}$	243	0.61	... (...)
IC110907A	55,811.795	$196.08^{+3.91}_{-2.68}$	$9.40^{+1.55}_{-1.06}$	186	0.51	4FGL J1301.6+0834 (1.06)
IC110929A	55,833.260	$121.45^{+1.34}_{-1.29}$	$50.04^{+0.24}_{-0.15}$	158	0.52	... (...)
IC110930A	55,834.445	$267.01^{+1.19}_{-1.14}$	$-4.44^{+0.60}_{-0.79}$	160	0.43	... (...)
IC111012A	55,846.867	$172.13^{+1.40}_{-1.39}$	$44.70^{+0.79}_{-0.45}$	115	0.43	... (...)
IC111120A	55,885.961	$26.06^{+1.89}_{-3.16}$	$9.82^{+1.40}_{-1.36}$	159	0.42	... (...)
IC111120B*	55,885.973	$356.84^{+0.53}_{-0.62}$	$-11.99^{+0.23}_{-0.27}$	4969	0.29	... (...)
IC111208A	55,903.719	$165.19^{+7.03}_{-4.13}$	$38.49^{+3.67}_{-3.49}$	123	0.45	4FGL J1101.5+3904 (0.6)
IC111209A	55,904.457	$99.98^{+1.19}_{-2.02}$	$20.42^{+1.60}_{-2.02}$	108	0.34	3HWC J0633+191 (1.95)
IC111213A	55,908.398	$247.85^{+1.71}_{-1.58}$	$0.56^{+1.46}_{-1.42}$	164	0.41	4FGL J1638.0+0042 (1.67)
IC111216A	55,911.277	$36.74^{+1.80}_{-2.24}$	$18.88^{+2.46}_{-2.82}$	891	0.95	SWIFT J0225.0+18 (0.46)
IC111218A	55,913.335	$26.85^{+3.69}_{-4.66}$	$7.03^{+4.04}_{-5.20}$	157	0.40	3FHL J0151.0+0539 (1.64)
IC120301A	55,987.807	$237.96^{+0.53}_{-0.62}$	$18.76^{+0.47}_{-0.51}$	433	0.82	... (...)
IC120426A	56,043.415	$183.56^{+2.15}_{-2.02}$	$0.52^{+0.86}_{-0.71}$	109	0.27	... (...)
IC120501A	56,048.570	$165.37^{+7.01}_{-5.36}$	$-71.51^{+3.53}_{-2.68}$	85	0.46	... (...)
IC120515A	56,062.959	$198.94^{+1.71}_{-1.41}$	$32.00^{+0.97}_{-1.09}$	194	0.61	... (...)
IC120523A	56,070.574	$171.08^{+0.66}_{-1.41}$	$26.44^{+0.46}_{-0.37}$	213	0.53	... (...)
IC120523A	56,070.639	$343.78^{+4.92}_{-4.48}$	$15.48^{+2.38}_{-1.54}$	168	0.49	4FGL J2253.9+1609 (0.72)
IC120529A	56,076.543	$176.48^{+6.64}_{-5.93}$	$22.87^{+2.70}_{-1.77}$	126	0.42	SWIFT J1141.3+21 (1.45)
IC120601A	56,079.306	$119.31^{+2.02}_{-0.92}$	$14.79^{+0.62}_{-0.73}$	137	0.40	... (...)
IC120605A	56,083.655	$152.58^{+1.89}_{-2.42}$	$36.38^{+1.54}_{-1.47}$	107	0.39	4FGL J1011.6+3600 (0.45)
IC120611A*	56,089.364	$39.95^{+0.26}_{-0.26}$	$-15.09^{+0.19}_{-0.31}$	9220	0.24	... (...)
IC120807A	56,146.207	$330.07^{+0.83}_{-0.83}$	$1.42^{+0.60}_{-0.45}$	373	0.74	... (...)
IC120916A	56,186.305	$182.24^{+1.36}_{-1.71}$	$3.88^{+0.67}_{-0.82}$	174	0.44	4FGL J1204.8+0407 (1.06)
IC120922A	56,192.549	$70.62^{+1.49}_{-1.27}$	$19.79^{+0.91}_{-0.71}$	143	0.43	... (...)
IC121011A	56,211.771	$205.14^{+0.66}_{-0.70}$	$-2.28^{+0.52}_{-0.56}$	481	0.84	... (...)
IC121026A	56,226.599	$169.80^{+1.32}_{-1.41}$	$27.91^{+0.85}_{-0.88}$	961	0.93	... (...)
IC121103A	56,234.508	$123.18^{+0.92}_{-0.97}$	$6.05^{+0.64}_{-0.56}$	112	0.28	... (...)
IC121115A	56,246.330	$225.70^{+1.01}_{-1.19}$	$8.88^{+0.94}_{-0.95}$	116	0.32	... (...)
IC130125A	56,317.266	$7.67^{+6.46}_{-5.92}$	$74.14^{+3.36}_{-2.82}$	165	0.53	4FGL J0028.1+7505 (0.97)
IC130125A	56,317.659	$280.46^{+1.89}_{-2.33}$	$-1.90^{+0.93}_{-0.82}$	114	0.31	4FGL J1847.2–0141 (1.37)
IC130127A	56,319.280	$352.97^{+1.32}_{-1.01}$	$-1.98^{+0.97}_{-0.90}$	235	0.61	4FGL J2333.4–0133 (0.58)
IC130208A*	56,331.121	$48.38^{+0.31}_{-0.31}$	$-13.32^{+0.23}_{-0.23}$	2268	0.32	... (...)
IC130316A	56,367.736	$303.41^{+2.98}_{-3.55}$	$54.68^{+1.77}_{-1.59}$	105	0.38	SWIFT J2006.5+56 (1.93)
IC130318A	56,369.285	$13.45^{+0.79}_{-0.88}$	$20.62^{+1.44}_{-0.99}$	106	0.33	... (...)
IC130408A	56,390.189	$167.83^{+2.64}_{-3.96}$	$20.66^{+1.28}_{-0.99}$	65	0.53	SWIFT J1114.3+20 (0.71)
IC130408B	56,390.758	$7.38^{+4.88}_{-8.04}$	$4.22^{+4.73}_{-3.58}$	163	0.40	4FGL J0030.4+0451 (0.68)
IC130409A	56,391.982	$163.56^{+2.68}_{-2.50}$	$29.44^{+4.38}_{-3.46}$	115	0.41	GB6 J1058+2817 (1.48)
IC130508A	56,420.641	$337.76^{+3.21}_{-2.02}$	$26.24^{+2.69}_{-1.90}$	140	0.45	SWIFT J2237.0+25 (1.35)
IC130509A	56,421.186	$317.50^{+1.76}_{-1.85}$	$2.09^{+1.19}_{-1.34}$	105	0.25	4FGL J2104.7+0108 (1.63)
IC130519A	56,431.483	$45.35^{+3.12}_{-1.49}$	$23.85^{+1.15}_{-0.89}$	110	0.36	... (...)
IC130531A	56,443.557	$164.18^{+2.42}_{-2.15}$	$6.32^{+1.32}_{-1.27}$	143	0.35	... (...)
IC130627A	56,470.110	$93.74^{+1.01}_{-1.14}$	$14.17^{+1.23}_{-1.04}$	851	0.94	4FGL J0615.9+1416 (0.26)
IC130627A	56,470.426	$155.35^{+3.87}_{-2.37}$	$3.73^{+1.72}_{-1.42}$	122	0.31	... (...)
IC130711A	56,484.530	$77.87^{+2.59}_{-1.19}$	$-2.43^{+1.34}_{-1.12}$	165	0.43	4FGL J0515.5–0125 (1.44)
IC130731A	56,504.072	$122.87^{+2.29}_{-4.35}$	$6.32^{+3.24}_{-2.40}$	122	0.32	4FGL J0812.5+0711 (0.92)
IC130801A	56,505.256	$214.98^{+4.35}_{-4.00}$	$7.75^{+1.24}_{-1.20}$	110	0.28	SWIFT J1419.1+07 (0.26)
IC130804A	56,508.815	$129.02^{+1.14}_{-1.54}$	$13.36^{+1.08}_{-1.68}$	113	0.33	... (...)
IC130808A	56,512.340	$26.59^{+1.14}_{-1.23}$	$9.22^{+0.91}_{-0.87}$	111	0.29	... (...)

Table 2
(Continued)

Alert	MJD	R.A. (deg)	Decl. (deg)	Energy (TeV)	Signalness	Nearest Source (deg)
IC130822A	56,526.409	$91.32^{+1.19}_{-1.19}$	$0.56^{+0.78}_{-0.63}$	115	0.30	3FHL J0604.9+0000 (0.56)
IC130907A*	56,542.793	$130.17^{+0.48}_{-0.31}$	$-10.54^{+0.27}_{-0.30}$	890	0.32	... (...)
IC131014A	56,579.909	$32.92^{+0.88}_{-0.70}$	$10.28^{+0.42}_{-0.57}$	293	0.67	... (...)
IC131023A	56,588.559	$301.90^{+1.01}_{-1.05}$	$11.61^{+1.14}_{-1.29}$	211	0.59	... (...)
IC131108A	56,604.553	$342.73^{+1.54}_{-1.58}$	$41.81^{+1.40}_{-0.89}$	153	0.50	... (...)
IC131112A	56,608.031	$129.24^{+0.26}_{-0.26}$	$-17.27^{+0.16}_{-0.16}$	7006	0.27	... (...)
IC131124A	56,620.145	$285.16^{+2.20}_{-1.54}$	$19.47^{+1.43}_{-1.46}$	180	0.55	... (...)
IC131204A	56,630.470	$288.98^{+1.10}_{-0.83}$	$-14.21^{+0.77}_{-1.31}$	259	0.20	4FGL J1916.7–1516 (1.08)
IC140101A	56,658.404	$192.26^{+2.07}_{-2.37}$	$-2.69^{+1.01}_{-0.71}$	200	0.56	4FGL J1251.3–0201 (0.88)
IC140103A	56,660.886	$37.90^{+25.61}_{-27.30}$	$78.97^{+5.86}_{-9.97}$	125	0.42	4FGL J0226.9+7744 (1.25)
IC140108A	56,665.308	$344.66^{+0.53}_{-0.48}$	$1.57^{+0.37}_{-0.34}$	214	0.69	... (...)
IC140109A	56,666.503	$293.12^{+0.79}_{-1.19}$	$33.02^{+0.45}_{-0.53}$	924	0.93	SWIFT J1933.9+32 (0.31)
IC140114A	56,671.878	$337.59^{+0.57}_{-0.92}$	$0.71^{+0.97}_{-0.86}$	54	0.34	4FGL J2227.9+0036 (0.61)
IC140122A	56,679.147	$138.82^{+3.52}_{-10.11}$	$37.45^{+1.95}_{-2.09}$	131	0.46	SWIFT J0920.1+37 (0.99)
IC140122B	56,679.204	$220.29^{+8.94}_{-8.37}$	$-86.07^{+0.59}_{-0.64}$	374	0.82	... (...)
IC140203A	56,691.785	$349.58^{+2.64}_{-2.55}$	$-13.55^{+1.15}_{-1.73}$	685	0.13	... (...)
IC140213A	56,701.809	$202.59^{+4.79}_{-3.21}$	$13.06^{+2.31}_{-2.52}$	140	0.39	4FGL J1326.1+1232 (1.14)
IC140223A	56,711.920	$118.83^{+11.87}_{-11.87}$	$32.58^{+5.68}_{-9.83}$	119	0.43	4FGL J0752.2+3313 (0.92)
IC140307A	56,723.920	$308.06^{+2.68}_{-4.61}$	$32.93^{+2.71}_{-3.23}$	109	0.40	4FGL J2028.3+3331 (1.01)
IC140324A	56,740.089	$225.70^{+5.67}_{-4.65}$	$51.06^{+4.00}_{-2.87}$	109	0.40	4FGL J1456.0+5051 (1.08)
IC140410A	56,757.099	$2.11^{+151.51}_{-58.92}$	$81.22^{+8.00}_{-6.94}$	246	0.63	SWIFT J0017.1+81 (0.5)
IC140411A	56,758.567	$146.95^{+3.12}_{-3.12}$	$15.91^{+2.89}_{-2.62}$	156	0.45	4FGL J0949.2+1749 (1.95)
IC140420A	56,767.859	$6.28^{+7.03}_{-5.89}$	$16.57^{+4.77}_{-5.11}$	163	0.49	4FGL J0023.9+1603 (0.58)
IC140503A	56,780.957	$162.30^{+6.91}_{-11.26}$	$46.57^{+5.41}_{-5.11}$	109	0.40	3FHL J1053.6+4930 (3.03)
IC140603A	56,811.142	$9.71^{+0.62}_{-0.88}$	$7.56^{+0.53}_{-0.83}$	152	0.38	... (...)
IC140609A	56,817.636	$106.26^{+2.68}_{-2.15}$	$1.31^{+1.05}_{-0.86}$	459	0.81	... (...)
IC140611A	56,819.204	$110.65^{+0.53}_{-0.62}$	$11.45^{+0.19}_{-0.19}$	5960	1.00	... (...)
IC140704A	56,842.298	$157.07^{+4.69}_{-4.64}$	$53.62^{+3.35}_{-3.48}$	150	0.50	SWIFT J1033.8+52 (1.07)
IC140705A	56,843.669	$25.88^{+1.85}_{-2.99}$	$2.54^{+1.79}_{-1.75}$	212	0.56	4FGL J0138.5+0300 (1.33)
IC140707A	56,845.500	$240.86^{+3.08}_{-2.07}$	$14.17^{+1.54}_{-1.65}$	167	0.48	4FGL J1606.2+1346 (0.8)
IC140713A	56,851.557	$0.79^{+1.14}_{-1.19}$	$15.60^{+0.89}_{-0.66}$	134	0.39	... (...)
IC140721A	56,859.759	$101.82^{+6.77}_{-6.86}$	$-32.89^{+5.23}_{-8.08}$	157	0.56	4FGL J0649.5–3139 (1.32)
IC140820A	56,889.378	$271.45^{+3.43}_{-1.80}$	$1.87^{+1.42}_{-1.46}$	108	0.27	... (...)
IC140923A	56,923.721	$169.72^{+0.70}_{-0.83}$	$-1.60^{+0.52}_{-0.30}$	209	0.24	... (...)
IC140927A	56,927.161	$50.89^{+3.91}_{-5.14}$	$-0.63^{+1.49}_{-1.42}$	182	0.48	3FHL J0323.6–0109 (0.54)
IC141012A	56,942.751	$63.85^{+2.24}_{-1.36}$	$3.21^{+0.90}_{-1.08}$	173	0.44	4FGL J0412.3+0239 (0.94)
IC141110A	56,971.297	$253.43^{+0.83}_{-1.10}$	$6.43^{+0.71}_{-0.68}$	113	0.29	... (...)
IC141114A	56,975.257	$221.48^{+4.53}_{-2.29}$	$28.00^{+2.31}_{-2.30}$	110	0.38	3FHL J1449.5+2745 (0.84)
IC141208A	56,999.668	$246.36^{+1.76}_{-1.89}$	$17.23^{+1.29}_{-1.09}$	109	0.33	4FGL J1626.4+1820 (1.13)
IC141210A	57,001.848	$318.12^{+2.33}_{-1.93}$	$1.57^{+1.57}_{-1.72}$	154	0.37	... (...)
IC141221A	57,012.410	$179.08^{+0.88}_{-1.10}$	$-1.94^{+0.71}_{-0.82}$	134	0.35	... (...)
IC150102A	57,024.796	$318.74^{+3.96}_{-1.27}$	$2.91^{+0.34}_{-0.49}$	126	0.32	... (...)
IC150104A	57,026.399	$272.11^{+1.71}_{-1.54}$	$28.76^{+2.41}_{-1.86}$	133	0.45	4FGL J1807.1+2822 (0.48)
IC150118A	57,040.509	$152.53^{+1.54}_{-2.72}$	$4.33^{+0.71}_{-0.86}$	156	0.37	... (...)
IC150119A	57,041.369	$286.92^{+1.36}_{-1.27}$	$6.43^{+0.60}_{-0.53}$	140	0.35	3HWC J1908+063 (0.14)
IC150120A	57,042.985	$95.89^{+1.19}_{-1.36}$	$14.13^{+0.50}_{-0.50}$	113	0.34	... (...)
IC150127A	57,049.481	$100.37^{+1.36}_{-1.63}$	$4.59^{+0.79}_{-0.67}$	293	0.66	... (...)
IC150129A	57,051.227	$358.51^{+3.91}_{-6.55}$	$6.39^{+3.16}_{-3.67}$	130	0.33	4FGL J2349.4+0534 (1.41)
IC150224A	57,078.000	$237.75^{+8.26}_{-2.26}$	$55.11^{+3.38}_{-3.03}$	106	0.38	4FGL J1553.1+5438 (0.56)
IC150313A	57,094.321	$127.05^{+1.76}_{-2.07}$	$-3.36^{+0.75}_{-0.75}$	107	0.29	... (...)
IC150428A	57,140.591	$31.07^{+4.04}_{-6.42}$	$15.02^{+1.94}_{-1.42}$	109	0.32	4FGL J0204.8+1513 (0.26)
IC150515A	57,157.942	$91.49^{+0.92}_{-0.75}$	$12.14^{+0.53}_{-0.50}$	401	0.77	... (...)
IC150526A	57,168.017	$139.79^{+2.46}_{-2.99}$	$-1.49^{+0.90}_{-1.01}$	108	0.28	4FGL J0914.1–0202 (1.36)
IC150601A	57,174.018	$333.37^{+2.42}_{-1.71}$	$9.63^{+1.21}_{-1.17}$	106	0.27	... (...)
IC150609A	57,182.027	$49.53^{+1.10}_{-1.10}$	$0.30^{+0.45}_{-0.82}$	118	0.31	... (...)
IC150609B	57,182.180	$245.43^{+1.67}_{-1.23}$	$0.22^{+1.04}_{-0.93}$	116	0.30	4FGL J1625.1–0020 (1.03)
IC150625A	57,198.640	$71.89^{+4.35}_{-4.70}$	$0.86^{+2.39}_{-1.83}$	112	0.29	4FGL J0442.6–0017 (1.69)

Table 2
(Continued)

Alert	MJD	R.A. (deg)	Decl. (deg)	Energy (TeV)	Signalness	Nearest Source (deg)
IC150625B	57,198.732	$306.43^{+2.02}_{-2.02}$	$19.08^{+0.91}_{-1.18}$	154	0.46	4FGL J2030.9+1935 (1.34)
IC150714A	57,217.910	$326.29^{+1.49}_{-1.32}$	$26.36^{+1.89}_{-2.19}$	439	0.84	... (...)
IC150809A*	57,243.322	$221.75^{+0.31}_{-0.26}$	$-17.15^{+0.23}_{-0.16}$	11667	0.20	... (...)
IC150812A	57,246.318	$317.59^{+5.10}_{-4.66}$	$30.09^{+2.31}_{-2.43}$	125	0.44	3FHL J2115.2+2933 (1.19)
IC150812B	57,246.759	$328.27^{+0.75}_{-0.88}$	$6.17^{+0.49}_{-0.53}$	508	0.83	... (...)
IC150823A	57,257.623	$325.90^{+3.47}_{-4.17}$	$-2.35^{+2.61}_{-2.09}$	133	0.35	4FGL J2148.9–0121 (1.66)
IC150831A	57,265.218	$54.76^{+0.92}_{-0.92}$	$34.00^{+1.13}_{-1.21}$	181	0.58	... (...)
IC150904A	57,269.760	$133.77^{+0.53}_{-0.88}$	$28.08^{+0.51}_{-0.55}$	302	0.74	3FHL J0854.1+2752 (0.29)
IC150914A	57,279.875	$129.68^{+1.89}_{-2.59}$	$30.35^{+1.88}_{-1.29}$	120	0.43	SWIFT J0840.2+29 (0.63)
IC150918A	57,283.546	$49.83^{+2.50}_{-3.74}$	$-2.95^{+1.35}_{-1.34}$	105	0.28	SWIFT J0324.9–03 (1.41)
IC150919A	57,284.206	$279.54^{+1.76}_{-2.29}$	$30.35^{+2.19}_{-1.50}$	228	0.67	4FGL J1836.4+3137 (1.32)
IC150923A	57,288.027	$103.23^{+0.70}_{-1.14}$	$3.96^{+0.60}_{-0.75}$	216	0.33	... (...)
IC150926A	57,291.901	$194.55^{+0.79}_{-1.23}$	$-4.56^{+0.93}_{-0.64}$	216	0.30	4FGL J1258.7–0452 (0.34)
IC151013A	57,308.124	$178.72^{+1.11}_{-1.15}$	$52.37^{+1.11}_{-1.11}$	156	0.52	... (...)
IC151017A	57,312.676	$197.53^{+2.46}_{-2.72}$	$19.95^{+3.01}_{-2.29}$	321	0.75	4FGL J1311.8+2057 (1.09)
IC151114A	57,340.873	$76.16^{+1.36}_{-1.36}$	$12.71^{+0.65}_{-0.73}$	1124	0.96	... (...)
IC151122A	57,348.532	$262.05^{+0.88}_{-1.05}$	$-2.24^{+0.63}_{-0.67}$	253	0.64	... (...)
IC160104A	57,391.444	$79.41^{+0.83}_{-0.75}$	$5.00^{+0.86}_{-0.97}$	217	0.57	4FGL J0515.9+0537 (0.75)
IC160128A	57,415.183	$263.76^{+1.10}_{-1.80}$	$-14.90^{+1.08}_{-1.20}$	583	0.15	... (...)
IC160225A	57,443.880	$311.87^{+2.18}_{-1.78}$	$60.06^{+1.65}_{-1.37}$	188	0.60	... (...)
IC160307A	57,454.697	$91.32^{+7.08}_{-8.66}$	$10.47^{+2.74}_{-4.45}$	106	0.28	4FGL J0608.6+1149 (1.59)
IC160331A	57,478.565	$151.22^{+0.66}_{-0.66}$	$15.48^{+0.66}_{-0.73}$	492	0.85	... (...)
IC160410A	57,488.735	$235.63^{+1.23}_{-1.45}$	$-4.07^{+1.31}_{-0.86}$	131	0.37	... (...)
IC160427A	57,505.245	$240.29^{+0.44}_{-0.48}$	$9.71^{+0.57}_{-0.42}$	85	0.45	... (...)
IC160510A	57,518.664	$352.88^{+1.76}_{-1.45}$	$1.90^{+0.75}_{-0.67}$	208	0.39	... (...)
IC160612A	57,551.434	$16.52^{+0.88}_{-0.18}$	$4.67^{+1.87}_{-0.52}$	106	0.25	... (...)
IC160614A	57,553.526	$214.76^{+3.16}_{-4.13}$	$40.82^{+3.33}_{-3.98}$	112	0.41	4FGL J1421.1+3859 (1.87)
IC160615A	57,554.404	$304.32^{+1.63}_{-1.05}$	$12.64^{+1.33}_{-1.34}$	150	0.41	4FGL J2014.9+1225 (0.61)
IC160707A	57,576.168	$351.43^{+1.54}_{-2.29}$	$0.60^{+0.82}_{-1.12}$	110	0.28	4FGL J2326.2+0113 (0.64)
IC160720A	57,589.914	$60.25^{+10.72}_{-8.88}$	$29.23^{+5.32}_{-5.87}$	108	0.37	4FGL J0358.1+2850 (0.74)
IC160727A	57,596.344	$113.12^{+1.93}_{-1.54}$	$14.67^{+1.08}_{-1.12}$	105	0.30	... (...)
IC160731A	57,600.080	$214.58^{+0.53}_{-0.57}$	$-0.30^{+0.45}_{-0.67}$	98	0.44	... (...)
IC160731A	57,600.785	$312.63^{+3.74}_{-3.21}$	$20.07^{+2.56}_{-2.13}$	118	0.39	4FGL J2043.9+2051 (1.73)
IC160806A	57,606.515	$122.78^{+0.88}_{-1.23}$	$-0.71^{+0.56}_{-0.56}$	219	0.58	... (...)
IC160812A	57,612.684	$86.99^{+15.29}_{-15.29}$	$48.83^{+9.95}_{-10.00}$	160	0.53	4FGL J0553.5+4810 (1.14)
IC160814A	57,614.907	$200.04^{+3.12}_{-2.68}$	$-32.13^{+1.75}_{-1.24}$	263	0.61	SWIFT J1325.2–32 (1.25)
IC160924A	57,655.741	$241.13^{+4.92}_{-5.89}$	$1.34^{+3.40}_{-2.80}$	191	0.51	4FGL J1608.4+0055 (1.07)
IC161001A	57,662.439	$192.57^{+2.50}_{-2.07}$	$37.12^{+1.51}_{-2.49}$	204	0.64	4FGL J1249.8+3707 (0.09)
IC161012A	57,673.613	$190.06^{+2.20}_{-4.04}$	$-7.48^{+2.18}_{-2.98}$	759	0.25	SWIFT J1239.6–05 (2.14)
IC161021A	57,682.309	$121.42^{+2.64}_{-2.90}$	$23.72^{+1.93}_{-2.02}$	135	0.43	4FGL J0803.0+2439 (1.12)
IC161027A	57,688.570	$119.00^{+2.94}_{-2.24}$	$1.53^{+2.32}_{-2.39}$	155	0.38	... (...)
IC161103A	57,695.380	$40.87^{+1.05}_{-0.57}$	$12.52^{+1.15}_{-0.61}$	85	0.31	4FGL J0244.7+1316 (0.82)
IC161117A	57,709.332	$78.66^{+1.85}_{-1.93}$	$1.60^{+1.90}_{-1.79}$	190	0.50	... (...)
IC161125A	57,717.430	$140.01^{+2.15}_{-1.19}$	$-0.11^{+0.75}_{-0.86}$	161	0.40	... (...)
IC161127A	57,719.665	$257.55^{+36.46}_{-29.23}$	$73.27^{+5.71}_{-9.96}$	139	0.45	4FGL J1651.6+7219 (1.66)
IC161210A	57,732.838	$46.36^{+2.37}_{-0.92}$	$15.25^{+0.93}_{-1.08}$	80	0.38	... (...)
IC161224A	57,746.537	$61.79^{+2.50}_{-2.37}$	$17.78^{+1.46}_{-1.56}$	139	0.42	SWIFT J0413.3+16 (1.69)
IC170105A	57,758.142	$309.95^{+5.01}_{-7.56}$	$8.16^{+2.00}_{-3.34}$	198	0.54	SWIFT J2033.1+09 (2.41)
IC170206A	57,790.549	$180.35^{+5.23}_{-3.82}$	$33.20^{+1.85}_{-2.16}$	135	0.46	4FGL J1205.8+3321 (0.94)
IC170208A	57,792.128	$99.67^{+2.59}_{-3.30}$	$16.84^{+1.60}_{-1.55}$	151	0.43	3HWC J0634+165 (1.14)
IC170208A	57,792.595	$92.81^{+1.23}_{-1.05}$	$4.59^{+0.94}_{-1.16}$	133	0.33	... (...)
IC170227A	57,811.065	$205.09^{+1.89}_{-3.96}$	$4.26^{+1.09}_{-1.12}$	108	0.27	SWIFT J1338.2+04 (0.59)
IC170308A	57,820.925	$155.35^{+2.02}_{-1.19}$	$5.53^{+0.98}_{-0.90}$	107	0.25	4FGL J1019.7+0511 (0.53)
IC170321A	57,833.314	$98.26^{+1.32}_{-0.92}$	$-15.06^{+1.04}_{-1.20}$	231	0.24	... (...)
IC170422A	57,865.646	$240.95^{+3.34}_{-5.71}$	$5.53^{+0.83}_{-1.01}$	161	0.39	... (...)
IC170427A	57,870.314	$5.32^{+4.48}_{-5.27}$	$-0.60^{+1.75}_{-1.23}$	155	0.38	3FHL J0022.0+0006 (0.73)
IC170514A	57,887.175	$311.97^{+2.20}_{-1.23}$	$18.60^{+2.10}_{-1.10}$	109	0.34	... (...)

Table 2
(Continued)

Alert	MJD	R.A. (deg)	Decl. (deg)	Energy (TeV)	Signalness	Nearest Source (deg)
IC170514B	57,887.300	$227.37^{+1.23}_{-1.10}$	$30.65^{+1.40}_{-0.99}$	174	0.55	... (...)
IC170527A	57,900.070	$178.59^{+2.77}_{-3.47}$	$26.49^{+3.82}_{-3.45}$	124	0.42	4FGL J1148.5+2629 (1.3)
IC170621A	57,925.191	$74.97^{+7.25}_{-7.78}$	$25.08^{+5.57}_{-6.20}$	109	0.37	SWIFT J0502.4+24 (0.68)
IC170626A	57,930.519	$280.99^{+3.03}_{-1.63}$	$8.80^{+1.13}_{-0.90}$	201	0.55	4FGL J1846.3+0919 (0.8)
IC170704A	57,938.293	$230.45^{+1.67}_{-1.71}$	$23.36^{+1.10}_{-0.89}$	195	0.60	... (...)
IC170717A	57,951.818	$208.39^{+1.67}_{-1.19}$	$25.16^{+1.41}_{-1.35}$	534	0.87	... (...)
IC170803A	57,968.084	$1.10^{+4.48}_{-1.76}$	$4.63^{+0.41}_{-0.41}$	214	0.56	... (...)
IC170809A	57,974.597	$21.27^{+0.75}_{-1.05}$	$-2.28^{+0.60}_{-0.67}$	226	0.60	... (...)
IC170819A	57,984.276	$26.98^{+1.85}_{-3.03}$	$18.88^{+1.11}_{-1.10}$	167	0.51	... (...)
IC170824A	57,989.554	$41.92^{+3.03}_{-3.56}$	$12.37^{+1.46}_{-1.30}$	175	0.49	SWIFT J0248.3+12 (0.38)
IC170922A	58,018.871	$77.43^{+1.14}_{-0.75}$	$5.79^{+0.64}_{-0.41}$	264	0.63	3FHL J0509.4+0542 (0.11)
IC170923A	58,019.021	$173.45^{+2.37}_{-2.55}$	$-2.54^{+0.90}_{-1.31}$	202	0.56	... (...)
IC171006A	58,032.308	$132.63^{+1.41}_{-2.24}$	$17.23^{+1.06}_{-0.66}$	118	0.37	... (...)
IC171015A	58,041.066	$162.91^{+2.99}_{-1.71}$	$-15.48^{+1.62}_{-1.98}$	72	0.55	SWIFT J1051.2–170 (1.58)
IC171028A	58,054.765	$294.52^{+3.56}_{-3.38}$	$2.05^{+2.20}_{-3.21}$	133	0.34	3FHL J1927.5+0153 (2.64)
IC171106A	58,063.778	$340.14^{+0.62}_{-0.62}$	$7.44^{+0.30}_{-0.26}$	1573	0.97	... (...)
IC171108A*	58,065.755	$269.65^{+0.22}_{-0.18}$	$-20.70^{+0.16}_{-0.16}$	20310	0.18	... (...)
IC180117A	58,135.752	$206.10^{+1.19}_{-1.14}$	$3.92^{+0.71}_{-0.78}$	85	0.42	... (...)
IC180123A	58,141.677	$77.12^{+2.50}_{-2.90}$	$8.01^{+0.41}_{-0.49}$	416	0.79	... (...)
IC180125A	58,143.976	$207.51^{+1.01}_{-0.57}$	$23.77^{+0.57}_{-0.57}$	110	0.36	... (...)
IC180205A	58,154.004	$17.40^{+1.36}_{-0.92}$	$-10.54^{+0.76}_{-0.72}$	113	0.23	... (...)
IC180213A	58,162.378	$66.97^{+2.46}_{-2.59}$	$6.09^{+1.95}_{-1.72}$	111	0.27	4FGL J0427.3+0504 (1.02)
IC180228A	58,177.572	$294.79^{+1.85}_{-1.71}$	$26.40^{+0.79}_{-1.12}$	124	0.42	... (...)
IC180313A	58,190.679	$287.18^{+0.75}_{-2.46}$	$5.53^{+0.34}_{-0.26}$	160	0.39	... (...)
IC180314A	58,191.804	$58.71^{+1.89}_{-1.67}$	$0.78^{+1.01}_{-1.01}$	145	0.36	... (...)
IC180316A	58,193.243	$271.71^{+1.19}_{-3.43}$	$-1.42^{+1.23}_{-1.27}$	156	0.39	4FGL J1759.0–0107 (1.97)
IC180410A	58,218.777	$218.50^{+0.79}_{-1.27}$	$0.56^{+0.75}_{-0.71}$	234	0.60	... (...)
IC180417A	58,225.279	$305.73^{+3.60}_{-1.58}$	$-4.41^{+0.67}_{-0.75}$	202	0.58	... (...)
IC180528A	58,266.506	$312.14^{+1.41}_{-2.02}$	$0.30^{+0.86}_{-1.45}$	110	0.28	4FGL J2049.7–0036 (0.97)
IC180608A	58,277.597	$69.08^{+1.63}_{-1.41}$	$-1.08^{+0.78}_{-0.78}$	158	0.40	4FGL J0436.2–0038 (0.43)
IC180612A	58,281.190	$338.69^{+5.10}_{-5.71}$	$3.73^{+2.81}_{-3.70}$	107	0.25	SWIFT J2235.7+01 (2.12)
IC180613A	58,282.982	$38.06^{+5.84}_{-4.26}$	$11.53^{+4.15}_{-4.91}$	155	0.41	4FGL J0231.8+1322 (1.84)
IC180728A*	58,327.845	$74.14^{+0.44}_{-0.35}$	$-17.74^{+0.51}_{-0.59}$	16952	0.18	... (...)
IC180807A	58,337.202	$100.37^{+4.00}_{-5.05}$	$11.15^{+2.98}_{-2.12}$	106	0.28	4FGL J0642.4+1048 (0.41)
IC180908A	58,369.833	$144.98^{+1.49}_{-2.20}$	$-2.39^{+1.16}_{-1.12}$	144	0.30	... (...)
IC180909A	58,370.604	$141.37^{+1.05}_{-1.27}$	$26.94^{+0.88}_{-1.00}$	171	0.53	... (...)
IC180919A	58,380.065	$258.40^{+1.49}_{-1.49}$	$32.84^{+0.94}_{-0.75}$	144	0.48	4FGL J1714.6+3228 (0.43)
IC181008A	58,399.779	$77.08^{+2.68}_{-3.56}$	$1.23^{+1.23}_{-1.16}$	108	0.27	... (...)
IC181014A	58,405.495	$225.22^{+1.36}_{-2.64}$	$-34.95^{+1.22}_{-1.79}$	62	0.39	4FGL J1505.0–3433 (0.94)
IC181023A	58,414.693	$270.18^{+1.89}_{-1.71}$	$-8.42^{+1.13}_{-1.55}$	237	0.15	4FGL J1804.4–0852 (1.03)
IC181023B	58,414.736	$78.27^{+1.76}_{-0.92}$	$21.54^{+0.96}_{-0.93}$	136	0.43	... (...)
IC181114A	58,436.945	$6.02^{+1.63}_{-2.24}$	$18.84^{+0.87}_{-0.98}$	145	0.44	... (...)
IC181120A	58,442.709	$25.71^{+5.54}_{-5.27}$	$11.72^{+2.41}_{-4.50}$	188	0.54	4FGL J0150.9+1230 (2.13)
IC181120B	58,442.944	$324.58^{+7.74}_{-9.04}$	$51.74^{+6.75}_{-9.48}$	173	0.57	SWIFT J2133.6+51 (0.94)
IC181121A	58,443.580	$132.19^{+7.34}_{-6.99}$	$32.93^{+4.19}_{-3.57}$	209	0.65	SWIFT J0848.1+34 (1.81)
IC181212A	58,464.085	$316.41^{+1.85}_{-2.02}$	$-31.00^{+1.68}_{-1.58}$	162	0.46	4FGL J2112.5–3043 (1.51)
IC190113A	58,496.089	$56.91^{+1.63}_{-1.41}$	$-0.82^{+0.75}_{-0.82}$	156	0.39	... (...)
IC190124A	58,507.155	$307.44^{+0.53}_{-1.14}$	$-32.22^{+0.96}_{-0.31}$	157	0.74	... (...)
IC190201A	58,515.016	$245.08^{+0.75}_{-0.88}$	$38.78^{+0.77}_{-0.67}$	163	0.53	... (...)
IC190214A	58,528.673	$228.25^{+0.79}_{-0.53}$	$-4.14^{+0.37}_{-0.30}$	348	0.74	... (...)
IC190221A	58,535.351	$268.59^{+1.41}_{-1.58}$	$-17.00^{+1.24}_{-0.51}$	56	0.55	... (...)
IC190223A	58,537.850	$155.21^{+0.70}_{-0.66}$	$19.67^{+0.28}_{-0.44}$	168	0.51	... (...)
IC190317A	58,559.832	$81.25^{+5.89}_{-5.98}$	$3.21^{+3.93}_{-4.07}$	108	0.26	3FHL J0521.6+0104 (2.3)
IC190410A	58,583.436	$310.61^{+3.30}_{-3.65}$	$12.22^{+2.84}_{-2.28}$	105	0.28	4FGL J2044.0+1036 (1.66)
IC190413A	58,586.450	$219.33^{+0.70}_{-1.32}$	$11.72^{+0.72}_{-0.72}$	107	0.29	4FGL J1438.6+1205 (0.49)
IC190413B	58,586.665	$245.57^{+1.23}_{-1.49}$	$21.98^{+1.21}_{-1.44}$	115	0.38	... (...)
IC190415A	58,588.437	$154.86^{+2.94}_{-4.70}$	$5.27^{+2.48}_{-1.95}$	117	0.30	4FGL J1019.7+0511 (0.11)

Table 2
(Continued)

Alert	MJD	R.A. (deg)	Decl. (deg)	Energy (TeV)	Signalness	Nearest Source (deg)
IC190422A	58,595.250	$166.90^{+3.21}_{-3.03}$	$17.39^{+2.00}_{-2.56}$	170	0.51	4FGL J1112.4+1751 (1.24)
IC190503A	58,606.724	$120.19^{+0.66}_{-0.66}$	$6.43^{+0.68}_{-0.75}$	142	0.34	... (...)
IC190504A	58,607.768	$65.17^{+1.67}_{-1.14}$	$-37.26^{+0.61}_{-1.09}$	55	0.39	3FHL J0420.4–3744 (0.48)
IC190515A	58,618.451	$127.88^{+0.79}_{-0.83}$	$12.60^{+0.50}_{-0.46}$	457	0.82	... (...)
IC190613A	58,647.829	$312.19^{+0.66}_{-0.79}$	$26.57^{+0.75}_{-0.71}$	195	0.61	... (...)
IC190619A	58,653.552	$343.52^{+4.13}_{-3.16}$	$10.28^{+2.02}_{-2.76}$	199	0.55	SWIFT J2254.2+114 (1.49)
IC190629A	58,663.809	$29.12^{+39.68}_{-118.65}$	$84.56^{+4.66}_{-4.40}$	109	0.34	3FHL J0249.7+8434 (1.26)
IC190704A	58,668.784	$161.81^{+2.15}_{-3.91}$	$26.90^{+1.94}_{-1.91}$	155	0.49	4FGL J1049.8+2741 (0.97)
IC190712A	58,676.052	$76.64^{+5.23}_{-6.99}$	$12.75^{+4.79}_{-2.82}$	109	0.30	4FGL J0502.5+1340 (1.34)
IC190730A	58,694.869	$226.14^{+1.27}_{-1.98}$	$10.77^{+1.03}_{-1.17}$	298	0.67	3FHL J1504.3+1030 (0.27)
IC190819A	58,714.732	$148.54^{+2.29}_{-3.30}$	$1.45^{+0.93}_{-0.75}$	113	0.29	3FHL J0946.2+0104 (2.01)
IC190922A	58,748.405	$167.30^{+2.81}_{-2.72}$	$-22.27^{+3.39}_{-3.31}$	3114	0.20	3FHL J1103.6–2328 (1.77)
IC190922B	58,748.961	$5.71^{+1.19}_{-1.27}$	$-1.53^{+0.90}_{-0.78}$	187	0.50	... (...)
IC191001A	58,757.840	$313.99^{+6.94}_{-2.46}$	$12.79^{+1.65}_{-1.64}$	218	0.59	4FGL J2052.7+1218 (0.91)
IC191119A	58,806.043	$229.31^{+5.49}_{-4.97}$	$3.77^{+2.47}_{-2.24}$	177	0.45	4FGL J1521.1+0421 (1.15)
IC191122A	58,809.948	$27.03^{+1.98}_{-2.72}$	$0.07^{+1.08}_{-1.57}$	127	0.33	... (...)
IC191204A	58,821.949	$80.16^{+2.42}_{-1.98}$	$2.87^{+1.05}_{-0.97}$	130	0.33	... (...)
IC191215A	58,832.465	$286.83^{+2.27}_{-1.92}$	$58.45^{+2.08}_{-1.86}$	133	0.48	... (...)
IC191231A	58,848.458	$48.47^{+5.98}_{-7.65}$	$20.11^{+4.48}_{-3.73}$	156	0.46	4FGL J0312.7+2012 (0.28)
IC200109A	58,857.987	$165.45^{+3.60}_{-4.39}$	$11.80^{+1.18}_{-1.29}$	375	0.77	3FHL J1103.1+1156 (0.35)
IC200117A	58,865.464	$116.02^{+0.79}_{-1.19}$	$29.18^{+0.86}_{-0.81}$	108	0.38	SWIFT J0744.0+29 (0.09)
IC200120A*	58,868.784	$67.41^{+0.40}_{-0.31}$	$-14.59^{+0.23}_{-0.27}$	6055	0.31	... (...)
IC200410A	58,949.972	$242.58^{+10.20}_{-10.20}$	$11.61^{+7.83}_{-6.19}$	110	0.30	SWIFT J1608.8+12 (0.78)
IC200421A	58,960.025	$87.93^{+3.43}_{-2.81}$	$8.23^{+2.08}_{-1.81}$	127	0.33	... (...)
IC200425A	58,964.977	$99.97^{+4.76}_{-3.00}$	$53.72^{+2.25}_{-1.69}$	135	0.48	SWIFT J0645.9+53 (1.14)
IC200512A	58,981.314	$295.18^{+1.67}_{-2.24}$	$15.79^{+1.24}_{-1.28}$	109	0.32	... (...)
IC200523A	58,992.104	$338.64^{+9.98}_{-6.02}$	$1.75^{+1.79}_{-3.51}$	105	0.25	SWIFT J2235.7+01 (0.3)
IC200530A	58,999.330	$255.37^{+2.46}_{-2.55}$	$26.61^{+2.32}_{-3.25}$	82	0.59	4FGL J1702.2+2642 (0.2)
IC200614A	59,014.529	$33.84^{+4.79}_{-6.37}$	$31.61^{+2.71}_{-2.25}$	115	0.41	4FGL J0220.2+3246 (1.57)
IC200615A	59,015.618	$142.95^{+1.14}_{-1.41}$	$3.66^{+1.16}_{-1.01}$	496	0.83	... (...)
IC200620A	59,020.127	$162.11^{+0.62}_{-0.92}$	$11.95^{+0.61}_{-0.46}$	114	0.33	... (...)
IC200806A	59,067.577	$157.25^{+1.17}_{-0.87}$	$47.75^{+0.64}_{-0.59}$	107	0.40	... (...)
IC200911A	59,103.597	$51.11^{+4.39}_{-10.99}$	$38.11^{+2.31}_{-1.97}$	111	0.41	SWIFT J0333.3+37 (1.94)
IC200916A	59,108.861	$109.78^{+1.05}_{-1.41}$	$14.36^{+0.85}_{-0.81}$	110	0.32	... (...)
IC200921A	59,113.797	$195.29^{+2.33}_{-1.71}$	$26.24^{+1.46}_{-1.73}$	117	0.41	3FHL J1303.0+2435 (1.7)
IC200926A	59,118.329	$96.46^{+0.70}_{-0.53}$	$-4.33^{+0.60}_{-0.75}$	670	0.44	... (...)
IC200926B	59,118.941	$184.75^{+3.65}_{-1.54}$	$32.93^{+1.16}_{-0.88}$	121	0.43	... (...)
IC200929A	59,121.742	$29.53^{+0.53}_{-0.53}$	$3.47^{+0.71}_{-0.34}$	183	0.47	... (...)
IC201007A	59,129.918	$265.17^{+0.48}_{-0.48}$	$5.34^{+0.30}_{-0.19}$	683	0.89	... (...)
IC201014A	59,136.093	$221.22^{+0.97}_{-1.19}$	$14.44^{+0.66}_{-0.46}$	147	0.41	... (...)
IC201021A	59,143.276	$260.82^{+1.71}_{-1.67}$	$14.55^{+1.31}_{-0.69}$	105	0.30	... (...)
IC201114A	59,167.629	$105.73^{+0.92}_{-1.27}$	$5.87^{+1.05}_{-1.01}$	214	0.56	... (...)
IC201115A	59,168.088	$195.12^{+1.23}_{-1.45}$	$1.38^{+1.27}_{-1.08}$	177	0.46	... (...)
IC201120A	59,173.406	$307.66^{+5.19}_{-5.68}$	$40.72^{+5.02}_{-2.75}$	154	0.50	4FGL J2032.6+4053 (0.41)
IC201130A	59,183.848	$30.54^{+1.10}_{-1.27}$	$-12.10^{+1.14}_{-1.11}$	203	0.15	4FGL J0206.4–1151 (1.07)
IC201209A	59,192.428	$6.86^{+1.01}_{-1.19}$	$-9.25^{+0.94}_{-1.10}$	419	0.19	... (...)
IC201221A	59,204.526	$261.69^{+2.28}_{-2.46}$	$41.81^{+1.25}_{-1.14}$	175	0.56	... (...)
IC201222A	59,205.039	$206.37^{+0.88}_{-0.75}$	$13.44^{+0.54}_{-0.34}$	186	0.53	... (...)

Note. The distance to the coincident sources is shown in parentheses with each source name. Events marked with an asterisk also triggered IceTop and are likely due to cosmic-ray showers. The errors on R.A. and decl. correspond to the 90% uncertainty likelihood contours (see text).

(This table is available in machine-readable form.)

6. Summary and Conclusion

Neutrinos play an extremely important role in the era of multimessenger astronomy, serving as our windows into the complex physics underlying cosmic-ray accelerators. To this end, IceCube has an active program dedicated to immediately alerting the community of a potential astrophysical neutrino detection. The program began in 2016, with significant

Table 3

The Number of Alerts with a Particular Catalog Source Located within the Error Contours, and the Number of Such Observations Expected due to Chance

Catalog	Observed Coincidences	Expected Coincidences
4FGL	119	140
3FHL	67	77
3HWC	8	6
TeVCat	12	16
BAT	66	73

improvements following in 2019 that are described in this work. Here we provide a catalog, the IceCube Event Catalog of Alert Tracks (ICECAT-1), of 275 track-like neutrino events that retroactively pass the alert criteria from 2011 to 2020. The event information for each alert is available to the public in the form of FITS (Pence et al. 2010) files that include the complete likelihood profiles providing an accurate grasp on the spatial uncertainty. This catalog, as well as updates with additional alerts, can be found at 10.7910/DVN/SCRUCD. This format will also be introduced for future IceCube alerts in addition to the traditional GCN notice format mode of distribution. We have also explored the correlation of IceCube alerts with sources from very high energy gamma-ray and X-ray catalogs and find them consistent with chance expectation. Future IceCube analyses will more systematically explore the correlation of these alerts with blazars, as well as with other IceCube data on long and short timescales (Abbasi et al. 2021d, 2023b). Several observatories have dedicated programs to searching for electromagnetic counterparts of the IceCube real-time alerts, leading to the identification of potential sites of cosmic-ray acceleration (Dzhappuev et al. 2020; Plavin et al. 2020; Stein et al. 2021; Necker et al. 2022). Multiwavelength follow-up observations will also benefit from the information provided about IceCube alerts in this catalog. We also note that a revised reconstruction framework is in the works that will improve the angular errors for alerts in the future.

Acknowledgments

The IceCube collaboration acknowledges the significant contributions to this manuscript from Mehr Un Nisa. We also acknowledge support from the following: USA—U.S. National Science Foundation—Office of Polar Programs, U.S. National Science Foundation—Physics Division, U.S. National Science Foundation—EPSCoR, Wisconsin Alumni Research Foundation, Center for High Throughput Computing (CHTC) at the University of Wisconsin–Madison, Open Science Grid (OSG), Advanced Cyberinfrastructure Coordination Ecosystem: Services & Support (ACCESS), Frontera computing project at the Texas Advanced Computing Center, U.S. Department of Energy—National Energy Research Scientific Computing Center, Particle Astrophysics Research Computing Center at the University of Maryland, Institute for Cyber-Enabled Research at Michigan State University, and Astroparticle Physics Computational Facility at Marquette University; Belgium—Funds for Scientific Research (FRS-FNRS and FWO), FWO Odysseus and Big Science programs, and Belgian Federal Science Policy Office (Belspo); Germany—Bundesministerium für Bildung und Forschung (BMBF), Deutsche Forschungsgemeinschaft (DFG), Helmholtz Alliance for Astroparticle Physics (HAP), Initiative and Networking Fund of the Helmholtz Association, Deutsches Elektronen Synchrotron (DESY), and High Performance Computing Cluster of the RWTH Aachen; Sweden—Swedish Research Council, Swedish Polar Research Secretariat, Swedish National Infrastructure for Computing (SNIC), and Knut and Alice Wallenberg Foundation; European Union—EGI Advanced Computing for research; Australia—Australian Research Council; Canada—Natural Sciences and Engineering Research Council of Canada, Calcul Québec, Compute Ontario, Canada Foundation for Innovation, WestGrid, and Compute Canada; Denmark—Villum Fonden, Carlsberg Foundation, and European Commission; New Zealand—Marsden Fund; Japan—Japan Society for Promotion of Science (JSPS) and Institute for Global Prominent Research (IGPR) of Chiba University; Korea—National Research Foundation of Korea (NRF); Switzerland—Swiss National Science Foundation (SNSF); United Kingdom—Department of Physics, University of Oxford.

Appendix

Here we provide the all-sky distribution of alerts for all alert types in Figure 6. Figure 7 shows the true neutrino energies as a function of the observed energy in the detector for simulated alerts.

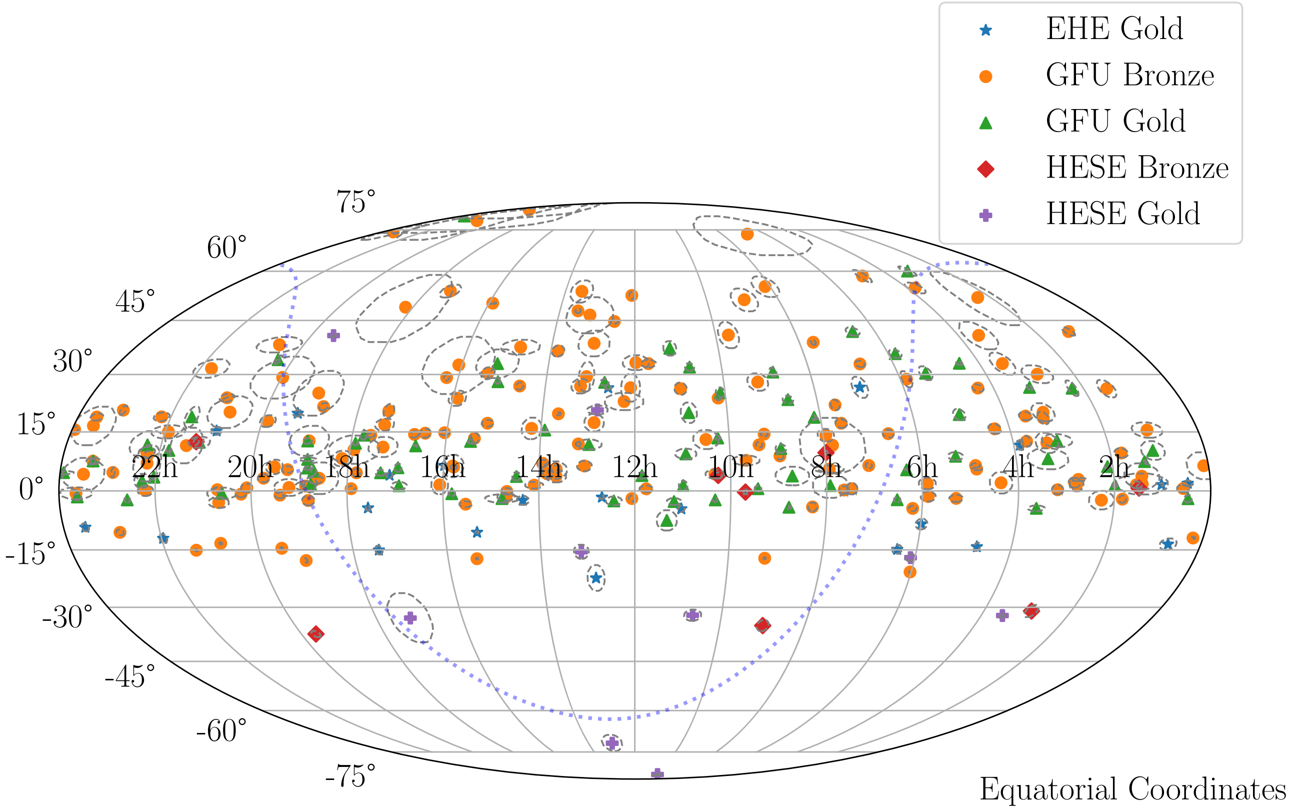

Figure 6. The all-sky distribution of the alerts in the catalog in equatorial coordinates. The blue stars denote EHE, the orange circles show GFU Bronze, the green triangles show GFU Gold, the red diamonds show HESE Bronze, and the purple plus signs show HESE Gold alerts. The 90% uncertainty contours at the location of each alert are shown by the dashed ellipses.

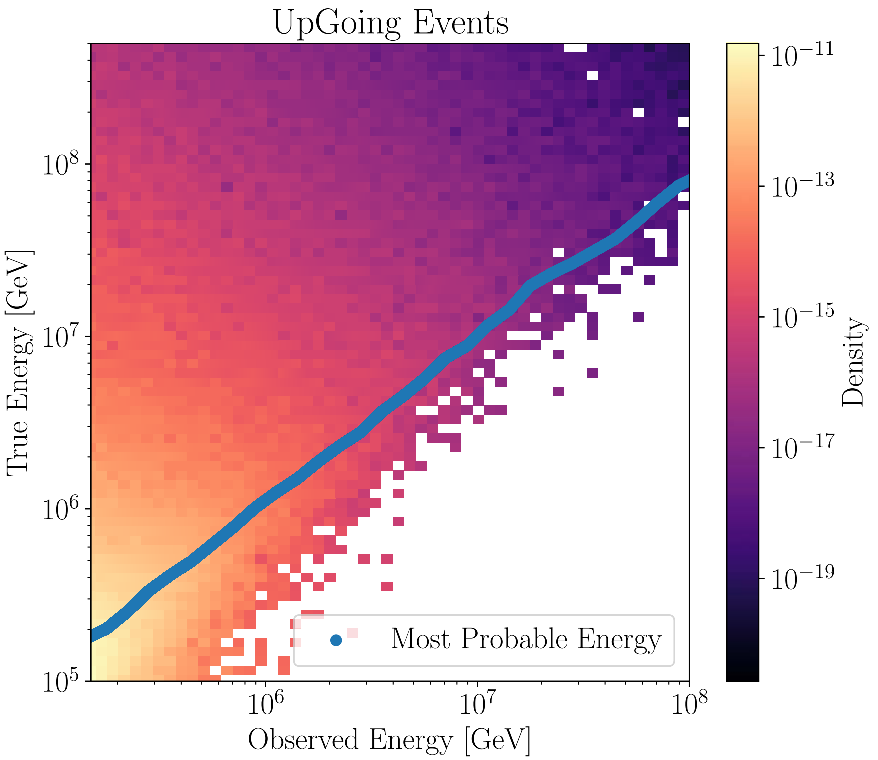

Figure 7. The true neutrino energy as a function of observed energy for simulated up-going GFU Gold events. The most likely estimated neutrino energy is shown in blue.

ORCID iDs

R. Abbasi https://orcid.org/0000-0001-6141-4205
M. Ackermann https://orcid.org/0000-0001-8952-588X
S. K. Agarwalla https://orcid.org/0000-0002-9714-8866
J. A. Aguilar https://orcid.org/0000-0003-2252-9514
M. Ahlers https://orcid.org/0000-0003-0709-5631
J. M. Alameddine https://orcid.org/0000-0002-9534-9189
G. Anton https://orcid.org/0000-0003-2039-4724
C. Argüelles https://orcid.org/0000-0003-4186-4182
Y. Ashida https://orcid.org/0000-0003-4136-2086
S. N. Axani https://orcid.org/0000-0001-8866-3826
X. Bai https://orcid.org/0000-0002-1827-9121
A. Balagopal V https://orcid.org/0000-0001-5367-8876
S. W. Barwick https://orcid.org/0000-0003-2050-6714
V. Basu https://orcid.org/0000-0002-9528-2009
J. J. Beatty https://orcid.org/0000-0003-0481-4952
J. Becker Tjus https://orcid.org/0000-0002-1748-7367
J. Beise https://orcid.org/0000-0002-7448-4189
C. Bellenghi https://orcid.org/0000-0001-8525-7515
S. BenZvi https://orcid.org/0000-0001-5537-4710
E. Bernardini https://orcid.org/0000-0003-3108-1141
E. Blaufuss https://orcid.org/0000-0001-5450-1757
S. Blot https://orcid.org/0000-0003-1089-3001
J. Y. Book https://orcid.org/0000-0001-6687-5959
C. Boscolo Meneguolo https://orcid.org/0000-0001-8325-4329
S. Böser https://orcid.org/0000-0002-5918-4890
O. Botner https://orcid.org/0000-0001-8588-7306
M. A. Campana https://orcid.org/0000-0003-4162-5739
C. Chen https://orcid.org/0000-0002-8139-4106
Z. Chen https://orcid.org/0000-0002-2813-7688
D. Chirkin https://orcid.org/0000-0003-4911-1345
B. A. Clark https://orcid.org/0000-0003-4089-2245
A. Coleman https://orcid.org/0000-0003-1510-1712
J. M. Conrad https://orcid.org/0000-0002-6393-0438
P. Coppin https://orcid.org/0000-0001-6869-1280
P. Correa https://orcid.org/0000-0002-1158-6735
D. F. Cowen https://orcid.org/0000-0003-4738-0787
P. Dave https://orcid.org/0000-0002-3879-5115
C. De Clercq https://orcid.org/0000-0001-5266-7059
J. J. DeLaunay https://orcid.org/0000-0001-5229-1995
D. Delgado https://orcid.org/0000-0002-4306-8828
H. Dembinski https://orcid.org/0000-0003-3337-3850
A. Desai https://orcid.org/0000-0001-7405-9994
P. Desiati https://orcid.org/0000-0001-9768-1858
K. D. de Vries https://orcid.org/0000-0002-9842-4068
G. de Wasseige https://orcid.org/0000-0002-1010-5100
T. DeYoung https://orcid.org/0000-0003-4873-3783
A. Diaz https://orcid.org/0000-0001-7206-8336
J. C. Díaz-Vélez https://orcid.org/0000-0002-0087-0693
H. Dujmovic https://orcid.org/0000-0003-1891-0718
M. A. DuVernois https://orcid.org/0000-0002-2987-9691
P. Eller https://orcid.org/0000-0001-6354-5209
P. A. Evenson https://orcid.org/0000-0001-7929-810X
K. L. Fan https://orcid.org/0000-0002-8246-4751
A. R. Fazely https://orcid.org/0000-0002-6907-8020
A. Fedynitch https://orcid.org/0000-0003-2837-3477
C. Finley https://orcid.org/0000-0003-3350-390X
D. Fox https://orcid.org/0000-0002-3714-672X
A. Franckowiak https://orcid.org/0000-0002-5605-2219
T. K. Gaisser https://orcid.org/0000-0003-4717-6620
E. Ganster https://orcid.org/0000-0003-4393-6944
A. Garcia https://orcid.org/0000-0002-8186-2459
A. Ghadimi https://orcid.org/0000-0002-6350-6485
T. Glauch https://orcid.org/0000-0003-1804-4055
T. Glüsenkamp https://orcid.org/0000-0002-2268-9297
S. J. Gray https://orcid.org/0000-0003-2907-8306
S. Griswold https://orcid.org/0000-0002-7321-7513
P. Gutjahr https://orcid.org/0000-0001-7980-7285
A. Hallgren https://orcid.org/0000-0001-7751-4489
L. Halve https://orcid.org/0000-0003-2237-6714
F. Halzen https://orcid.org/0000-0001-6224-2417
H. Hamdaoui https://orcid.org/0000-0001-5709-2100
A. Haungs https://orcid.org/0000-0002-9638-7574
K. Helbing https://orcid.org/0000-0003-2072-4172
F. Henningsen https://orcid.org/0000-0002-0680-6588
C. Hill https://orcid.org/0000-0003-0647-9174
W. Hou https://orcid.org/0000-0003-3422-7185
T. Huber https://orcid.org/0000-0002-6515-1673
K. Hultqvist https://orcid.org/0000-0003-0602-9472
M. Hünnefeld https://orcid.org/0000-0002-2827-6522
G. S. Japaridze https://orcid.org/0000-0002-7000-5291
M. Jin https://orcid.org/0000-0003-0487-5595
B. J. P. Jones https://orcid.org/0000-0003-3400-8986
D. Kang https://orcid.org/0000-0002-5149-9767
W. Kang https://orcid.org/0000-0003-3980-3778
A. Kappes https://orcid.org/0000-0003-1315-3711
T. Karg https://orcid.org/0000-0003-3251-2126
M. Karl https://orcid.org/0000-0003-2475-8951
A. Karle https://orcid.org/0000-0001-9889-5161
U. Katz https://orcid.org/0000-0002-7063-4418
M. Kauer https://orcid.org/0000-0003-1830-9076
J. L. Kelley https://orcid.org/0000-0002-0846-4542
A. Khatee Zathul https://orcid.org/0000-0002-8735-8579
A. Kheirandish https://orcid.org/0000-0001-7074-0539
J. Kiryluk https://orcid.org/0000-0003-0264-3133
S. R. Klein https://orcid.org/0000-0003-2841-6553
A. Kochocki https://orcid.org/0000-0003-3782-0128
R. Koirala https://orcid.org/0000-0002-7735-7169
H. Kolanoski https://orcid.org/0000-0003-0435-2524
T. Kontrimas https://orcid.org/0000-0001-8585-0933
C. Kopper https://orcid.org/0000-0001-6288-7637
D. J. Koskinen https://orcid.org/0000-0002-0514-5917
P. Koundal https://orcid.org/0000-0002-5917-5230
M. Kovacevich https://orcid.org/0000-0002-5019-5745
M. Kowalski https://orcid.org/0000-0001-8594-8666
A. Kumar https://orcid.org/0000-0002-8367-8401
N. Kurahashi https://orcid.org/0000-0003-1047-8094
C. Lagunas Gualda https://orcid.org/0000-0002-9040-7191
M. Lamoureux https://orcid.org/0000-0002-8860-5826
M. J. Larson https://orcid.org/0000-0002-6996-1155
F. Lauber https://orcid.org/0000-0001-5648-5930
J. P. Lazar https://orcid.org/0000-0003-0928-5025
J. W. Lee https://orcid.org/0000-0001-5681-4941
K. Leonard DeHolton https://orcid.org/0000-0002-8795-0601
A. Leszczyńska https://orcid.org/0000-0003-0935-6313
Q. R. Liu https://orcid.org/0000-0003-3379-6423
L. Lu https://orcid.org/0000-0003-3175-7770
F. Lucarelli https://orcid.org/0000-0002-9558-8788
A. Ludwig https://orcid.org/0000-0001-9038-4375
W. Luszczak https://orcid.org/0000-0003-3085-0674
Y. Lyu https://orcid.org/0000-0002-2333-4383
J. Madsen https://orcid.org/0000-0003-2415-9959
I. C. Mariş https://orcid.org/0000-0002-5771-1124
R. Maruyama https://orcid.org/0000-0003-2794-512X

F. McNally https://orcid.org/0000-0002-0785-2244
K. Meagher https://orcid.org/0000-0003-3967-1533
M. Meier https://orcid.org/0000-0002-9483-9450
L. Merten https://orcid.org/0000-0003-1332-9895
T. Montaruli https://orcid.org/0000-0001-5014-2152
R. W. Moore https://orcid.org/0000-0003-4160-4700
M. Moulai https://orcid.org/0000-0001-7909-5812
R. Naab https://orcid.org/0000-0003-2512-466X
R. Nagai https://orcid.org/0000-0001-7503-2777
J. Necker https://orcid.org/0000-0003-0280-7484
H. Niederhausen https://orcid.org/0000-0002-9566-4904
M. U. Nisa https://orcid.org/0000-0002-6859-3944
A. Obertacke Pollmann https://orcid.org/0000-0002-2492-043X
B. Oeyen https://orcid.org/0000-0003-2940-3164
E. O'Sullivan https://orcid.org/0000-0003-1882-8802
H. Pandya https://orcid.org/0000-0002-6138-4808
N. Park https://orcid.org/0000-0002-4282-736X
E. N. Paudel https://orcid.org/0000-0001-9276-7994
C. Pérez de los Heros https://orcid.org/0000-0002-2084-5866
S. Philippen https://orcid.org/0000-0002-0276-0092
A. Pizzuto https://orcid.org/0000-0002-8466-8168
M. Plum https://orcid.org/0000-0001-8691-242X
B. Pries https://orcid.org/0000-0003-4811-9863
A. Rehman https://orcid.org/0000-0001-7616-5790
E. Resconi https://orcid.org/0000-0003-0705-2770
W. Rhode https://orcid.org/0000-0003-2636-5000
B. Riedel https://orcid.org/0000-0002-9524-8943
M. Rongen https://orcid.org/0000-0002-7057-1007
C. Rott https://orcid.org/0000-0002-6958-6033
D. Ryckbosch https://orcid.org/0000-0002-8759-7553
I. Safa https://orcid.org/0000-0001-8737-6825
D. Salazar-Gallegos https://orcid.org/0000-0002-9312-9684
A. Sandrock https://orcid.org/0000-0002-6779-1172
M. Santander https://orcid.org/0000-0001-7297-8217
S. Sarkar https://orcid.org/0000-0002-1206-4330
S. Sarkar https://orcid.org/0000-0002-3542-858X
H. Schieler https://orcid.org/0000-0002-2637-4778
S. Schindler https://orcid.org/0000-0001-5507-8890
F. Schlüter https://orcid.org/0000-0002-5545-4363
J. Schneider https://orcid.org/0000-0001-7752-5700
F. G. Schröder https://orcid.org/0000-0001-8495-7210
L. Schumacher https://orcid.org/0000-0001-8945-6722
S. Sclafani https://orcid.org/0000-0001-9446-1219
S. Seunarine https://orcid.org/0000-0003-3272-6896
M. Silva https://orcid.org/0000-0001-6940-8184
B. Skrzypek https://orcid.org/0000-0002-0910-1057
B. Smithers https://orcid.org/0000-0003-1273-985X
D. Soldin https://orcid.org/0000-0003-3005-7879
G. Sommani https://orcid.org/0000-0002-0094-826X
G. M. Spiczak https://orcid.org/0000-0002-0030-0519
C. Spiering https://orcid.org/0000-0001-7372-0074
T. Stezelberger https://orcid.org/0000-0003-2676-9574
T. Stuttard https://orcid.org/0000-0001-7944-279X
G. W. Sullivan https://orcid.org/0000-0002-2585-2352
I. Taboada https://orcid.org/0000-0003-3509-3457
S. Ter-Antonyan https://orcid.org/0000-0002-5788-1369
W. G. Thompson https://orcid.org/0000-0003-2988-7998
K. Tollefson https://orcid.org/0000-0001-9725-1479
S. Toscano https://orcid.org/0000-0002-1860-2240
C. F. Tung https://orcid.org/0000-0001-6920-7841
M. A. Unland Elorrieta https://orcid.org/0000-0002-6124-3255
N. Valtonen-Mattila https://orcid.org/0000-0002-1830-098X
J. Vandenbroucke https://orcid.org/0000-0002-9867-6548
N. van Eijndhoven https://orcid.org/0000-0001-5558-3328
J. van Santen https://orcid.org/0000-0002-2412-9728
S. Verpoest https://orcid.org/0000-0002-3031-3206
T. B. Watson https://orcid.org/0000-0002-8631-2253
C. Weaver https://orcid.org/0000-0003-2385-2559
C. Wendt https://orcid.org/0000-0001-8076-8877
N. Whitehorn https://orcid.org/0000-0002-3157-0407
C. H. Wiebusch https://orcid.org/0000-0002-6418-3008
M. Wolf https://orcid.org/0000-0001-9991-3923
S. Yoshida https://orcid.org/0000-0003-2480-5105
T. Yuan https://orcid.org/0000-0002-7041-5872

References

Aartsen, M., Ackermann, M., Adams, J., et al. 2018a, Sci, 361, 147
Aartsen, M., Ackermann, M., Adams, J., et al. 2018b, Sci, 361, eaat1378
Aartsen, M. G., Abbasi, R., Abdou, Y., et al. 2013, Sci, 342, 1242856
Aartsen, M. G., Abbasi, R., Ackermann, M., et al. 2014a, JINST, 9, P03009
Aartsen, M. G., Abbasi, R., Ackermann, M., et al. 2021, Natur, 591, 220
Aartsen, M. G., Abraham, K., Ackermann, M., et al. 2016a, JINST, 11, P11009
Aartsen, M. G., Abraham, K., Ackermann, M., et al. 2016b, ApJ, 833, 3
Aartsen, M. G., Abraham, K., Ackermann, M., et al. 2017c, ApJ, 835, 151
Aartsen, M. G., Ackermann, M., Adams, J., et al. 2014b, PhRvL, 113, 101101
Aartsen, M. G., Ackermann, M., Adams, J., et al. 2015, EPJC, 75, 116
Aartsen, M. G., Ackermann, M., Adams, J., et al. 2017a, JINST, 12, P03012
Aartsen, M. G., Ackermann, M., Adams, J., et al. 2017b, APh, 92, 30
Aartsen, M. G., Ackermann, M., Adams, J., et al. 2019, ApJ, 886, 12
Aartsen, M. G., Ackermann, M., Adams, J., et al. 2020a, PhRvL, 125, 121104
Aartsen, M. G., Ackermann, M., Adams, J., et al. 2020b, PhRvL, 124, 051103
Abbasi, R., Abdou, Y., Ackermann, M., et al. 2013, NIMPA, 703, 190
Abbasi, R., Ackermann, M., Adams, J., et al. 2009, NIMPA, 601, 294
Abbasi, R., Abdou, Y., Abu-Zayyad, T., et al. 2011, PhRvD, 83, 012001
Abbasi, R., Abdou, Y., Abu-Zayyad, T., et al. 2012, APh, 35, 615
Abbasi, R., Abdou, Y., Ackermann, M., et al. 2013, NIMPA, 700, 188
Abbasi, R., Ackermann, M., Adams, J., et al. 2021a, PhRvD, 104, 022002
Abbasi, R., Ackermann, M., Adams, J., et al. 2021b, JINST, 16, P07041
Abbasi, R., Ackermann, M., Adams, J., et al. 2021c, Proc ICRC (Berlin), 37, 1045
Abbasi, R., Ackermann, M., Adams, J., et al. 2021d, ApJ, 910, 4
Abbasi, R., Ackermann, M., Adams, J., et al. 2022a, ApJ, 928, 50
Abbasi, R., Ackermann, M., Adams, J., et al. 2022b, TCD, submitted
Abbasi, R., Ackermann, M., Adams, J., et al. 2022c, ApJ, 926, 59
Abbasi, R., Ackermann, M., Adams, J., et al. 2023a, ApJ, 951, 45
Abbasi, R., Ackermann, M., Adams, J., et al. 2023b, ApJ, 954, 75
Abbott, B. P., Abbott, R., Abbott, T. D., et al. 2017, ApJL, 848, L12
Abdollahi, S., Acero, F., Ackermann, M., et al. 2020, ApJS, 247, 33
Ajello, M., Atwood, W. B., Baldini, L., et al. 2017, ApJS, 232, 18
Albert, A., Alfaro, R., Alvarez, C., et al. 2020, ApJ, 905, 76
Amin, N. M. B. 2021, JPhCS, 2156, 012217
Ayala Solares, H. A., et al. 2020, APh, 114, 68
Blaufuss, E., Kintscher, T., Lu, L., & Tung, C. F. 2020, Proc. ICRC (Madison), 36, 1021
Dzhappuev, D. D., et al. 2020, JETPL, 112, 753
Górski, K. M., Hivon, E., Banday, A. J., et al. 2005, ApJ, 622, 759
Haack, C., & Wiebusch, C. 2017, Proc. ICRC (Busan), 35, 1005
Heck, D., Knapp, J., Capdevielle, J. N., Schatz, G., & Thouw, T. 1998, CORSIKA: a Monte Carlo Code to Simulate Extensive Air Showers (Karlsruhe: Forschungszentrum Karlsruhe GmbH)
Kankare, E., Huber, M., Smartt, S. J., et al. 2019, A&A, 626, A117
Kronmueller, M., & Glauch, T. 2019, Proc. ICRC (Madison), 36, 937
Necker, J., de Jaeger, T., Stein, R., et al. 2022, MNRAS, 516, 2455
Oh, K., Koss, M., Markwardt, C. B., et al. 2018, ApJS, 235, 4
Pence, W. D., Chiappetti, L., Page, C. G., Shaw, R. A., & Stobie, E. 2010, A&A, 524, A42
Plavin, A., Kovalev, Y. Y., Kovalev, Y. A., & Troitsky, S. 2020, ApJ, 894, 101
Schönert, S., Gaisser, T. K., Resconi, E., & Schulz, O. 2009, PhRvD, 79, 043009
Stein, R., van Velzen, S., Kowalski, M., et al. 2021, NatAs, 5, 510
Wakely, S. P., & Horan, D. 2008, Proc. ICRC (Mérida), 30, 1341